# Renewable Energy Management System: Optimum Design and Hourly Dispatch

Baraa Mohandes ⬤, *Member, IEEE*, Maisam Wahbah ⬤, *Member, IEEE*,
Mohamed Shawky El Moursi ⬤, *Senior Member, IEEE*, and Tarek H.M. El-Fouly ⬤, *Senior Member, IEEE*

*Abstract*—This paper introduces a new framework for optimum design and operation of hybrid renewable energy plants (HREP) augmented with battery energy storage systems (BESS). A new renewable energy management system (REMS) is developed comprising three components: 1) Enhanced joint forecasting of wind and solar outputs based on deep neural networks and also multiplicative weights update (MWU); 2) an advanced optimization model for sizing the HREP-BESS components and the policy of BESS operation; and 3) Augmenting the rolling hourly dispatch for HREP-BESS with a novel dynamic ramping limit and a criterion for reduction of deviations from the hour-ahead dispatch schedule. The proposed REMS tool enables maintaining the inter-hourly ramping of the HREP-BESS output within a threshold. In this context, a novel dynamic ramp limit is proposed to minimize the energy curtailment during operation and maximize energy sales to the power grid. The advantage of the proposed REMS tool over the classical renewable energy systems operation scheme is the mitigation of the volatility of renewable energy sources (RES) by suppressing extreme ramping events with minimum curtailment. Moreover, the costs and revenues of the HREP-BESS design and operation are assessed over a 25 years period. The design problem is solved for different scenarios, and the optimal solution always encloses a hybrid mix of renewables where the share of the PV plant can reach up to 37.1% of the total plant size. With the proposed REMS, the curtailment of RES never exceeds 12.9% even when the HREP is operated without a reserve margin. For the selected design, the optimum BESS capacity is 12.9% of the HREP capacity. The number of hours which observe a ramping violation event is 2.4% of the season's length (2184 hours). 99% of all ramping events fall within the defined ramping limits. The use of the MWU method increases the total profit by 2.53% compared with adopting the average forecast.

*Index Terms*—Deep learning, multiplicative weights update, rolling horizon, hybrid renewable energy, dynamic ramping limit, proxy value of battery energy.

## NOMENCLATURE

### A. Set Indices

| | |
|---|---|
| $t$ | Hour of operations in a season $t \in \{1, \ldots, 2184\}$ |
| $\tau$ | Hours of the look-ahead horizon $\tau \in \{0, \ldots, 4\}$ in a provisional dispatch plan devised at each interval $t$ |
| $\kappa$ | Weather scenario $\kappa \in \mathcal{K}$ |

### B. Fixed Parameters

| | |
|---|---|
| $C_{\text{HREP}}$ | Total capacity of the hybrid RES plant $= 100$MW |
| $\pi_{(\cdot)}$ | Unit cost of $(\cdot)$ |
| $\eta_{\text{BESS}}$ | Round trip efficiency of BESS |
| $\zeta$ | Future uncertainty factor |

### C. Optimum Sizing & Design Decision Variables

| | |
|---|---|
| $\psi$ | Capacity of the PV unit as a percentage of $C_{\text{HREP}}$ |
| $1 - \psi$ | Capacity of the wind unit as a percentage of $C_{\text{HREP}}$ |
| $C_{\text{BESS}}$ | Capacity of the BESS as a percentage of $C_{\text{HREP}}$ |
| $\pi_{P_{\text{BESS}}}$ | Proxy price of the energy stored in the BESS (SoC) as a percentage of maximum energy price $\pi_E$ |

### D. Hourly Economic Dispatch Decision Variables

| | |
|---|---|
| $P_\tau^t$ | Power output of the HREP at hour $\tau$ of the look-ahead horizon, according to the provisional dispatch schedule devised at $t$ |
| $\rho_0^{\pm,t}$ | Actual power ramping between periods $t-1$ and $t$ |
| $\rho_\tau^{\pm,t}$ | Anticipated power ramping between periods $\tau - 1$ and $\tau$ in the provisional dispatch plan devised at $t$. $\tau > 1$ |
| $\hat{\rho}_0^{\pm,t}$ | Violation size of the tolerable ramping limit between period $t-1$ and $t$ |
| $\rho_\tau^{\pm,t}$ | Anticipated violation size of the tolerable ramping limit between periods $\tau - 1$ and $\tau$ in the provisional dispatch plan devised at $t$. $\tau > 1$ |
| $\delta^{\pm,t}$ | Deviation in actual HREP power output at $t$ from the provisional dispatch schedule devised at the previous time interval $t-1$. |

### E. Hourly Economic Dispatch Parameters

| | |
|---|---|
| $\widetilde{\rho}_0^{\pm,t}$ | Tolerable ramping limit of actual power output between periods $t-1$ and $t$ |

$\widetilde{\rho}_{\tau}^{\pm,t}$     Provisional tolerable ramping limit between periods $\tau - 1$ and $\tau$ in the provisional dispatch plan devised at $t$

## I. Introduction

RENEWABLE energy (RE) is gaining interest worldwide due to environmental concerns. New policies require grid operators to supply a certain percentage of their load from renewable energy sources (RES), or face high penalties. The biggest challenge for grid operators and area balancing authorities against integrating more RES is the volatility and uncertainty of RES output, inherited from the nature of weather conditions. Therefore, power system operators secure high amounts of operating reserve, usually through conventional generators [1].

Applied studies on actual RE data conclude that suppressing the drastic effects of RES on the power system requires large amounts of load-following reserves [1]–[5]. For example, Sørensen *et al.* [6] highlight that the most extreme drop in a wind farm's output within a 1-minute interval is 6% of the plant's rating. In contrast, the most extreme drop in a 10 minutes or 30 minutes period is 27% and 45%, respectively. Similarly, partial clouding of photovoltaic (PV) panels can decrease a PV plant's output by more than 50% within 1 h [7], [8]. Against all these findings, European grid codes [9]–[11] define ramping rate limits at the 1-minute time-frame only. The ramping limits are 1%–1.5% of the RES capacity subject to a maximum of 60 MW/min. Theoretically, this allows the RES owner to ramp continuously at the maximum rate for extended periods of time, without any legal repercussions. Consequently, the RES output is allowed within one hour to change by 60%–90% of the RES capacity, subject to a maximum of 3.6 GW. In practice, this would have a drastic effect on the grid, both technically and economically.

The lack of load-following resources on the part of slow large units has required fast small units to provide this necessary resource at a premium cost. This leads to more aggressive cycling of small thermal generators; a process characterized by lower fuel efficiency and higher physical stress on these units [1], [12], [13]. The consequent carbon emissions from aggressive cycling defeat the original purpose of installing renewable energy sources. Therefore, ramping reserve is an ever-present issue in research on RES integration. In fact, several researchers dedicated their effort to studying ramping reserve, in particular. The authors of [14], [15] highlight the shortcomings in the existing estimations of the ramping capability for thermal units, and the inter-period ramping process in hourly dispatch. Bakirtzis *et al.* [16] adopt a probabilistic method to determine the ramping reserve requirement, such that the reserve accommodates a percentage of all errors in forecasting the net-load. The authors analyze the impact of a more conservative reserve requirement (i.e. accommodating a bigger percentage of forecast errors) on the dispatch and operation costs.

The majority of existing studies focus on providing the system with more ramping reserve from thermal units, rather than mitigate the root cause of additional reserves, which is the RES variability. On the other hand, mitigation of RES variability on the RES side is limited to operating RES below their maximum power point tracking level, where this spare margin represents reserve against large fluctuations or forecast errors [17]–[19]. Hedayati-Mehdiabadi *et al.* [19] generate different wind-scenarios, and optimize the wind curtailment factor for each scenario offline, and a lookup table of curtailment policies is produced. During real-time operation, the actual weather conditions are compared against the generated wind scenario in the look-up table, and the closest scenario is determined, and its curtailment factor is applied, accordingly.

In addition, the majority of research in this area is focused on eliminating fluctuations at the time-frame of seconds to few minutes. For example, [20]–[22] optimize the operation of a RE plant augmented with a battery energy storage system (BESS) at time resolutions between seconds and 10-minutes, with a model predictive control approach. In [13], a single forecast of wind-speed for the next 1 minute is modeled as a Gaussian process, and operation of the wind/BESS plant is optimized as a two-stage decision recourse problem. For a PV/BESS plant in [8], the output of the next minute is modeled as a discrete-time Markov process and the plant's operation is optimized accordingly. Similar work on smoothing RES output is the subject of [23]–[25]. The statistical tools used in these studies are reliable only for making short-term predictions at the seconds–minutes timeframe. Due to the small size of fluctuations in the seconds–minutes period, BESS degradation is not studied in [8], [13], [21]–[26]. BESS degradation is also oversimplified in [27]–[29].

Proper sizing of BESS calls for observing the accumulation of fatigue, and the corresponding capacity depletion over the battery's life. For example, operating BESS at very low state of charge (SoC) inflicts severe damage on the BESS lifetime [30]–[33]. Battery degradation models which analyze the electrochemical reactions at molecular levels are the most accurate, however, these models are very complex. BESS fatigue accumulation models have acceptable accuracy, moderate complexity, and also incorporate multiple operation factors. A number of these models are presented in [31]–[33]. One of these models, the rainflow counting (RFC) algorithm has the ability to analyze non-regular cycling profiles.

Fewer studies optimize the hourly economic dispatch of RES plants. References [34]–[36] schedule system operations at varying time resolutions for the look-ahead period. The effect of time-resolution on system performance in light of wind volatility and uncertainty is discussed in [34]. Bakirtzis *et al.* [35] solve a deterministic optimization problem to schedule operations for multiple upcoming short periods incorporating security against contingencies. The dispatch during the remaining horizon (few hours - 36 hours) is planned using a larger time-period, and does not incorporate security constraints. A stochastic formulation incorporating the loss of load probability is adopted later in [36].

Ding *et al.* [37] optimize the operation of a wind farm with a BESS in the day-ahead market, based on 12-36 hours forecast. Instead of re-solving the optimization problem during real-time operation stage, the decision variables are updated with respect to the errors in wind power forecast and market price forecast, using an affine transformation. This transformation incurs lower computational burden than solving the optimization problem again. However, an affine transformation does not guarantee the optimality of the new solution in a nonlinear program, and BESS

degradation is not considered. Wang *et al.* [38] optimize the operation and bidding of a BESS for the next 48 hours period to maximize the BESS owner profits. The profits of the next day (24-48 hours) period are weighted down by a factor which is meant to represent uncertainty. However, a fixed discount factor is used without investigation. A constraint on the BESS state of charge (SoC) at the end of the present day is applied to support operations on the next day. The BESS degradation is incorporated in the optimization as a fixed cost on energy exchange only.

The predictability of a hybrid PV/Wind plant is twice that of any single RES alone [39]. Using hybrid RES plants for lower overall volatility is suggested in [39]–[41]. Hybrid renewable energy plants are studied by [7], [41]–[43]. Reddy *et al.* [7] optimize the operation of a hybrid renewable energy plant (HREP) aided by a diesel generator. Operations are scheduled in the DA market to minimize cost, and again in the HA market with the objective of minimizing the quadratic cost of deviation from the DA schedule. The operation objective also includes the cost and revenue from trading renewable-obligation certificates. The authors use a heuristic optimization algorithm to solve the problem, which may not scale up very well with a large system. A small HREP installation is sized to match a load profile in [42] for multiple objectives: minimize pollutant emissions, minimize social discomfort, and minimize costs. Energy in excess of the target load profile is penalized, rather than sold to the grid.

Anwar *et al.* [43] utilize an ensemble of nonlinear auto-regressive neural networks with exogenous inputs to make 30-minutes forecasts of wind and marine current speeds. The bootstrapping technique is employed to process the output of the neural-networks and create a prediction interval with 95% confidence level. The prediction interval demonstrates better performance than point-forecasts. The HREP's operation philosophy is to dispatch the wind turbines (WT) at their maximum available level, while controlling the marine-current turbine (MCT) and a BESS to satisfy a hard ramping constraint. The BESS is sized based on the largest deviation event, which turns out to be 5% of the total plant's capacity.

The following gaps can be outlined in the existing literature. The absence of any grid codes on maximum allowed ramping for RES units at the 30-60 minutes period indicates that the existing approach to RES integration is questionable. One of the outcomes of this paper is the recommendation to update grid-codes to apply a ramping limit at this time-frame. Moreover, smoothing RES output at the seconds–minutes time-frame does not supersede the need for optimizing RES operation at larger time steps (i.e. 30-60 minutes), for two reasons:

- First, the energy storage systems (ESS) employed in smoothing techniques have smaller size and different nature. Ultra-capacitors (UC) are used for smoothing in [8], however, UC cannot be employed for load-following reserve due to their small energy capacity.
- Secondly, it is impractical to limit the scheduling of the power system's operations to only a short look-ahead period of few minutes, despite the accuracy of these forecasts.

Therefore, this paper attempts to achieve the following requirements: A) maintain a steady output of RES without extreme ramping events as well as maintaining the RES output reasonable close to its forecast; and B) acquire better forecasts of RES output for a longer look-ahead horizon.

To satisfy requirement (A) in the plant design (long-term), the involvement level of BESS in arbitrage is optimized. Exploring the potential of commercial arbitrage requires analyzing the extent of its interference with the BESS's primary task of reducing power fluctuations, and also the effect of arbitrage on BESS aging. Consequently, this paper proposes a novel concept of a proxy value of stored BESS energy and using this value in operations scheduling. Moreover, the hybrid mix of RES is optimized while the total size of the HREP is fixed at 100MW.

Existing literature has little work on optimizing the HREP design based on the outputs of the hourly economic dispatch over extended periods of time. Therefore, requirement (A) is also tackled in short-term operations where the HREP operation philosophy adopts a "fine, do not confine" approach to suppress extreme ramping events. That is, the HREP's operation philosophy applies a dynamic soft-limit on the RES inter-hourly ramping and penalizes extreme ramping events rather than constrains them. Penalizing extreme ramping events plays the role of mitigating RES volatility. In this quest, different designs of the ramping soft-limit are investigated along with different penalty factors. Consequently, RES variability is attenuated on the RES side first, rather than exposing the central grid to its full extent and calling for procurement of massive amounts of reserve. A small penalty is also imposed on deviating from the provisional operation schedule devised in the hour-ahead market. Penalizing deviation from the HA-market plan plays the role of mitigating the uncertainty aspect of RES.

To fulfill requirement (B), an ensemble of deep neural networks is employed to generate a set of RES output forecasts. Later on, a machine-learning algorithm known as the multiplicative weights update (MWU), processes the set of forecasts into one forecast guaranteed to be better than or equivalent to the best single forecast alone.

This paper is organized as follows: The optimum HREP sizing and optimum hourly dispatch problems are formulated in Section II. Generating RES scenarios from probability distributions is discussed in Section III-A. The deep-learning technique and multiplicative weights update method are described in Section IV. The proposed test system is described in Section V. Results of the case study are discussed in Section VI, and Section VII concludes.

## II. METHODOLOGY AND PROBLEM FORMULATION

### A. Hourly Economic Dispatch

At each hour $t$, the actual dispatch of the HREP is denoted $P_0^t$, which is determined and deployed at the beginning of the hour. The actual ramping between the present and the previous hour is denoted $\rho_0^{\pm,t}$. At the same hour $t$, a provisional plan for the 4 hours of the look-ahead horizon is also devised, denoted $P_\tau^t$, $\tau \in \{1, \ldots, 4\}$. The anticipated ramping among hours in the look-ahead horizon in this provisional plan is denoted $\rho_\tau^{\pm,t}$. The
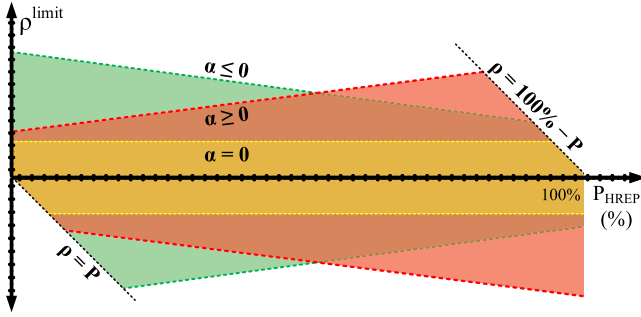
Fig. 1.     Dynamic ramp rate limit for different values of $\alpha$.



Fig. 2.     Nomenclature in the rolling/receding horizon dispatch.

superscript $t \in \{1, \ldots, 2184\}$ identifies hours of the season. $\tau \in \{0, 1, .., 4\}$ identifies hours in a dispatch plan. This nomenclature applies to all quantities in addition to $P$ and $\rho$ in dispatch plans. In this study, an enhanced hourly economic dispatch problem is proposed with three novel features.

First, in order to tackle the volatility aspect of RES output, it is desirable to suppress extreme ramping between any two consecutive hours of operation $\rho^{\pm,t}$. The (up, down) ramping is defined in (1). (2) defines the inter-hourly ramping limit $\tilde{\rho}$ for the HREP as the sum of a fraction $\alpha$ of the actual dispatch $P_0^{t-1}$ in the previous hour, and a fraction $\beta$ of the HREP's full capacity $C_{\text{HREP}}$. Consequently, $\alpha$ determines the dynamic component of the ramping limit, and $\beta$ sets a static component. The ramping limit criterion is usually implemented as a hard constraint shown in (iii), which may lead to severe curtailment or even infeasibility in extreme situations. Alternatively, a high penalty is enforced on on excessive ramping $\hat{\rho}$ in order implement a soft ramping limit. This is defined in (3). Either (iii) or (3) can be activated in an optimization problem. If both were activated, the hard-constraint (iii) subdues $\hat{\rho}$ in (3) to zero. Intuitively, this criterion is deactivated for the first hour in a season since $P_0^{-1}$ is undefined, (4).

It must be kept in mind that parameters $\{\alpha, \beta\}$ are out of control of the HREP operator, albeit, are dictated by the grid-code. The HREP must comply with this criterion or face harsh penalties. $\beta$ defines the fixed component of the ramping rate limit as a percentage of the HREP's full capacity. A value of $\beta = 0$ prevents the HREP from descending to, or rising up from zero. Therefore, it is crucial to set $\beta > 0$. $\alpha$ defines a flexible ramping limit which grows or shrinks with the HREP's power output. A value $\alpha < 0$ tightens the ramping limit around high output levels, with larger values of $|\alpha|$ applying a tighter limit. At the same time, a larger value of $\beta$ allows the HREP bigger ramping room to rise from low generation levels. Fig. 1 depicts the effect of different values of $\alpha$. It is important to choose values $(\alpha, \beta)$ that satisfy $-\alpha \leq \beta$. Otherwise, the ramping limit becomes negative at some point $P_{\text{HREP}} \leq 100\%$, which is undesirable. The lines $\rho = p$ and $\rho = 100\% - p$ represent the upper and lower limits of output power $P_{\text{min/max}}$, which also bound the plant's ramping near these bounds. For example, when $P_{\text{HREP}} = 10\%$, the HREP cannot ramp down by more than 10%, such that its output becomes negative. Similarly, when $P_{\text{HREP}} = 95\%$, the HREP cannot ramp up by more than 5%.
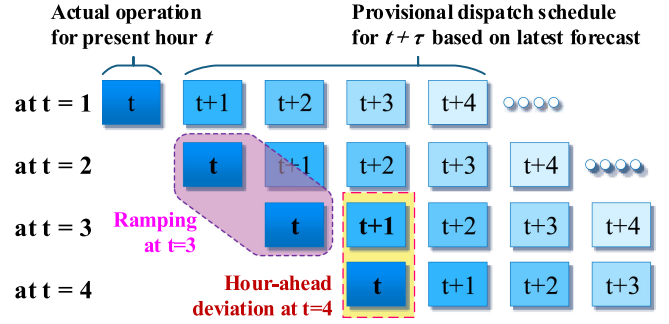
The second enhancement on the economic dispatch problem aims to tackle the uncertainty aspect of RES output by penalizing deviation from the HA schedule. Fig. 2 illustrates the difference between the inter-hour ramping $\rho$ and the deviation from the hour-ahead plan $\delta$. The provisional dispatch plan for $t$ devised in the previous hour $t-1$ is denoted $P_1^{t-1}$, and considered a binding agreement in the HA market. The difference between $P_0^t$ and $P_1^{t-1}$ is defined as the HA deviation $\delta^t$, and described in (5). This deviation might be inevitable, and may also be tolerable within a certain limit. Therefore, violating this criterion incurs a smaller penalty.

$$\rho_\tau^{\pm,t} = \begin{cases} \max\{0, \ P_0^t \mp P_0^{t-1}\} & \tau = 0 \\ \max\{0, \ P_\tau^t \mp P_{\tau-1}^t\} & \tau \in \{1, .., 4\} \end{cases} \tag{1}$$

$$\tilde{\rho}_\tau^t = \begin{cases} \alpha P_0^{t-1} + \beta C_{\text{HREP}} & \tau = 0 \\ \alpha P_{\tau-1}^t + \beta C_{\text{HREP}} & \tau \in \{1, .., 4\} \end{cases} \tag{2}$$

$$\rho_\tau^{\pm,t} \leq \tilde{\rho}_\tau^t \quad \text{Equation is printed for illustration only} \tag{iii}$$

$$\rho_\tau^{\pm,t} \leq \tilde{\rho}_\tau^t + \hat{\rho}_\tau^t \tag{3}$$

$$t = 0 \Rightarrow P_{(\cdot)}^{t-1} \text{ is u.d.} \Rightarrow \tilde{\rho}_0^t := \infty, \hat{\rho}_0^t := 0 \tag{4}$$

$$\delta^{\pm,t} = \max\{0, P_0^t \mp P_1^{t-1}\} \tag{5}$$

Involving BESS in arbitrage may interfere with its primary task of providing flexibility. If the BESS discharges completely in an arbitrage scheme, the BESS would fail to provide any energy to suppress a steep unpredicted ramp-down event, or a large HA-deviation. If the ramping penalty is very high, the potential financial profits from arbitrage are outweighed by the huge penalties. On the other hand, if the ramping-penalty is mediocre, the profits from arbitrage may justify the payment of ramping penalties. Therefore, the HREP operator should optimize the involvement extent of the BESS in arbitrage. In addition, aggressive cycling of the BESS has a drastic effect on the BESS state of health. BESS degradation depends on the depth of discharge of each charge-discharge cycle. Therefore, BESS degradation at any hour is dependent on a future event, and it cannot be incorporated during actual real-time operation.

The third enhancement in this study is the employment of a proxy value for the value of energy stored in the BESS $\pi_{\text{PBESS}}$. When this value is high, the HREP is more frugal towards

spending the BESS energy, and preserves BESS energy for suppressing extreme ramping events and avoiding the associated penalties. In contrast, when $\pi_{\text{PBESS}}$ is low, the HREP expends the BESS energy with more liberty. The proxy value of energy can be perceived in another way. When the power output of a BESS has a non-zero value, the system perceives the BESS as a potential generator and dispatchable load. The system would be willing to discharge the BESS only if the benefit from discharging the BESS exceeds the value of energy. On the other hand, the system would be willing to charge up the BESS only if the cost of charging the BESS is lower than the proxy value $\pi_{\text{P}_{\text{BESS}}}$.

The hourly dispatch problem is described by (6) – (14), in addition to (1) – (5). This problem is solved for the full season length of 2184 hours. At every hour $t$, the actual HREP dispatch $P_0^t$ is determined, and also a provisional dispatch plan for the look-ahead horizon of 4 hours is set. The decision variables of the problem are: the power output of the PV and WT sources, the power exchange of the BESS, the HA deviation, the actual ramping and excess ramping (if any) for the present hour and the look ahead horizon. The HREP sells its output to the grid at price $\pi_E^t$, and also pays a penalty rate $\pi_{\hat{\rho}}$ on the total excess ramping $\hat{\rho}_0^{\pm,t}$, and on deviation from the hour-ahead schedule $\delta^t$. The BESS acts as a generator with a non-negative cost $\pi_{\text{PBESS}}$. The net power output of the HREP is sold to the grid, as described by (7). Variables with undetermined sign are decomposed to positive and negative parts in ((1)), ((5)), and (8). The BESS SoC is updated in every period by (10), where $\eta_{\text{BESS}}$ is the BESS round-trip efficiency.

RES may be operated below their maximum power point, where this spare margin represents reserve against large fluctuations or forecast errors [17]–[19]. This criterion is described by (12), where the reserve margin can be defined as a fraction $\lambda$ of the available RES energy, or as a fixed value $\varphi$ in MW. In the optimization objective, revenues and penalties in the provisional plan for the look-ahead horizon are weighed down by a factor $(\zeta)^\tau, \zeta \in (0,1], \tau \in \{0,\ldots,4\}$. The coefficient $(\zeta)^\tau$ decays exponentially, thus, giving later hours a smaller weight. A similar principle is applied in [38] with a fixed factor.

$$\max \sum_{\tau}^{\{0,\ldots,4\}} \left[ \pi_E^{t+\tau} P_{\text{HREP},\tau}^t - \pi_E^{t+\tau} \pi_{\hat{\rho}} \hat{\rho}_\tau^t - \pi_{\text{PBESS}} P_{\text{BESS},\tau}^t \right]$$
$$\times (\zeta)^\tau - \pi_E^{t+\tau} \pi_\delta \delta^t, \qquad \pi_{\hat{\rho}}, \pi_\delta \in [200\%, 500\%] \qquad (6)$$

$$P_{\text{HREP},\tau} = P_{\text{WT},\tau} + P_{\text{PV},\tau} + P_{\text{BESS},\tau} \qquad \forall t \in \mathcal{T} \tag{7}$$

$$P_{\text{BESS},\tau}^t = P_{\text{BESS},\tau}^{+,t} + P_{\text{BESS},\tau}^{-,t} \qquad \forall t \in \mathcal{T} \tag{8}$$

$$P_{\text{BESS}}^{-,t} \leq 0 \leq P_{\text{BESS}}^{+,t} \qquad \forall t \in \mathcal{T} \tag{9}$$

$$\text{SoC}_0^t = \text{SoC}_0^{t-1} - P_{\text{BESS},0}^{\pm,t-1} \cdot (\eta_{\text{BESS}})^{\mp 1} \qquad \forall t \in \mathcal{T} \tag{10}$$

$$\text{SoC}_{\tau>0}^t = \text{SoC}_0^t - \sum^{\{0,\ldots,\tau-1\}} P_{\text{BESS},\tau}^{\pm,t} \cdot (\eta_{\text{BESS}})^{\mp 1} \quad \forall t \in \mathcal{T} \tag{11}$$

$$R_{\text{HREP},\tau} \geq \lambda \left( P_{\text{WT},\tau}^{\max,t} + P_{\text{PV},\tau}^{\max,t} \right) + \varphi \qquad \forall t \in \mathcal{T} \tag{12}$$

$$\left| P_{\text{BESS},\tau}^{\pm,t} \right| \leq P_{\text{BESS}}^{\max} \qquad \forall t \in \mathcal{T} \tag{13}$$

$$0 \leq \text{SoC}_\tau^{\min,t} \leq \text{SoC}_\tau^t \leq \text{SoC}_\tau^{\max,t} \qquad \forall t \in \mathcal{T} \tag{14}$$

### B. HREP Sizing and BESS Arbitrage Policy

After solving the hourly economic dispatch problem for every season, the rainflow counting (RFC) algorithm is applied on the BESS SoC profiles to evaluate the BESS degradation, and the BESS is oversized accordingly. The actual revenues and penalties in a financial analysis depend only on the actual dispatch at each period $P_0^t, \rho_0^t, \delta^t$, while quantities for the look-ahead horizon $P_\tau^t, \rho_\tau^t$ are only provisional for system operators. Similarly, the proxy value of BESS stored energy does not count towards the project's actual revenues and costs. The results of hourly-operations across all seasons and weather scenarios can be extrapolated to the whole project's lifetime $\overline{yr}$, and used to evaluate the goodness of a candidate design of the HREP. The optimum HREP design problem is described in (15) – (25). The decision variables of the design and sizing problem are: the PV and WT sizes, the BESS capacity $C_{\text{BESS}}$, and the proxy value of BESS energy $\pi_{\text{P}_{\text{BESS}}}$.

The objective function in (15) is the net present value of total profits over the project's lifetime. The decision variables of optimization are the PV unit size $\psi$, the BESS capacity $C_{\text{BESS}}$, the proxy value of BESS stored energy $\pi_{\text{P}_{\text{BESS}}}$, and the oversizing factor of the BESS $OvF_{\text{BESS}}$ to offset BESS degradation. The capital expenses comprise the cost of installation of the PV, WT, BESS and inverter, in (17). The HREP full capacity is assumed fixed, and the scope of optimization is finding the optimal mix of PV vs. WT in the HREP, denoted as $\psi$ and described by 19. The BESS inverter size depends on the magnitude of the largest power exchange action by the BESS (20). Operation expenses consist of: 1) The oversizing (i.e. derating) factor of the PV unit (OvF$_{\text{PV}}$), which denotes the additional PV units installed annually to offset PV degradation $\mathbb{D}_{\text{PV}}$, 2) The additional BESS units (OvF$_{\text{BESS}}$) installed annually to offset BESS degradation, described by (22). These expenses are deducted from the expected seasonal profits over all scenarios and seasons in (21). Net profits of every year are adjusted for interest and inflation $IR'$ [29]. The salvage value of all equipment at the end of the project's lifetime is represented by (24). The first term in (24) pertains to the equipment installed at the very beginning of the project whose age is $\overline{yr}$. The second term represents the value of equipment installed within the project's lifetime whose age is $\overline{yr} - yr$. At the end of the project lifetime, the equipment is sold for its salvage value $\mathbb{S}$.

The BESS degradation model in (25) is known as the exponential model [44]. The denominator implies that the BESS can go through 5135.7 full cycles (i.e. DoD=100%) before the BESS is considered dead. The RFC algorithm maps the cycling profile of a BESS into a list of full-cycles and half cycles. The equivalent depth of discharge (DoD) for each event is calculated,

and mapped into a percentage of damage to the BESS using (25).

$$\max_{\{\psi, C_{\text{BESS}}, \pi_{\text{PBESS}}\}} \begin{pmatrix} \frac{\mathbb{S}}{(1+IR')^{\overline{yr}}} - \text{CapEx} \\ + \sum^{yr} \frac{\text{Rev}-\text{OpEx}-\text{Pnt}}{(1+IR')^{yr}} \end{pmatrix} \tag{15}$$

$$IR' = \frac{IR - F}{F + 1} \tag{16}$$

$$\text{CapEx} = \pi_{\text{CPV}} \, \text{OvF}_{\text{PV}} \, C_{\text{PV}} + \pi_{\text{CWT}} \, C_{\text{WT}}$$
$$+ \pi_{\text{CBESS}} \, \text{OvF}_{\text{BESS}} \, C_{\text{BESS}} \, C_{\text{HREP}} + \pi_{\text{CInv}} \, C_{\text{Inv}} \tag{17}$$

$$C_{\text{PV}} = \psi \cdot C_{\text{HREP}} \tag{18}$$

$$C_{\text{WT}} = (1 - \psi) \cdot C_{\text{HREP}} \tag{19}$$

$$C_{\text{Inv}} \geq \max_{\{t,\kappa\}} \left| P_{\text{BESS}}^{t,\kappa} \right| \tag{20}$$

$$\text{Rev} = \mathbb{E}_\kappa \left[ \sum^t \pi_{\text{E}}^t \, P_{\text{HREP},0}^{t,\kappa} \right] \tag{21}$$

$$\text{OpEx} = \mathbb{E}_\kappa \left[ \pi_{\text{PV}} \, (\text{OvF}_{\text{PV}} - 1) \, C_{\text{PV}} \right.$$
$$\left. + \pi_{\text{BESS}} \, (\text{OvF}_{\text{BESS}} - 1) \, C_{\text{BESS}} \right] \tag{22}$$

$$\text{Pnt} = \mathbb{E}_\kappa \left[ \pi_{\hat{\rho}} \cdot \sum^t \hat{\rho}_0^{t,\kappa} + \pi_\delta \cdot \sum^t \delta^{t,\kappa} \right] \tag{23}$$

$$\mathbb{S} = (1-S)^{\overline{yr}}\text{CapEx} + \sum^{yr} \frac{(1-S)^{(\overline{yr}-yr)}}{(1+IR')^{yr}} \, \text{OpEx} \tag{24}$$

$$\mathbb{D}(\text{DoD}) = \frac{(\text{DoD})^{1.759}}{5135.7} \times 100\% \tag{25}$$

## III. WEATHER SCENARIO GENERATION

### A. Non-Parametric Probabilistic Modeling

Historical datasets for wind speed, solar irradiance, and ambient temperature from a location in France are used in developing the probabilistic models for the wind and PV power generation [45]. Nineteen years of data are divided into three seasons; winter, summer, and a combined fall-spring season. Then, the dataset for each season is further divided into eight time intervals of equal length: $\{< 0, 1, 2 >, < 3, 4, 5 >, \ldots, < 21, 22, 23 >\}$. With eight intervals per day for each of three seasons, twenty four subsets of data are created. For each set, two probability density functions (PDFs) are generated for the wind speed and solar irradiance data using a non-parametric Kernel Density Estimator (KDE).

Non-parametric techniques proved to be more efficient and accurate in probabilistic modeling of wind and solar data than traditional techniques such as the Rayleigh or Weibull distributions for wind speed and the Beta distribution for solar irradiance [46], [47]. The adopted KDE uses Unbiased Cross-Validation (UCV) for bandwidth selection in the rth derivative of the KDE "$f^{(r)}(x)$." The UCV bandwidth "$h$" is given by [48]:

$$\hat{h}_{ucv}^{(r)} = \underset{h^r}{arg\,min} \, UCV(h, r) \tag{26}$$

$$UCV(h; r) = \int \left( \hat{f}_h^{(r)}(x) \right)^2 dx - 2n^{-1}(-1)^r \sum_{i=1}^n \hat{f}_{h,i}^{(2r)} (X_i) \tag{27}$$

for $r = 0, 1, 2, \ldots$, which minimizes the function. The wind speed probabilistic model is based on the specifications of the VESTAS WT model $V82 - 1.65$ [49] with cut-in $v_{\text{in}}$, rated $v_{\text{rated}}$, and cut-out $v_{\text{out}}$ wind speeds of 3, 13, and 25 m/s, respectively. Wind speed data in each time interval dataset is sorted into 12 bins, where the speed range $v_{\text{in}}-v_{\text{rated}}$ is represented by 10 of the 12 states. The probability of occurrence of each state is calculated from the UCV PDF and the corresponding power of the state is calculated from:

$$P_w = \begin{cases} 0 & ; 0 \leq v_a < v_{\text{in}} \\ \frac{v_a - v_{\text{in}}}{v_{\text{rated}} - v_{\text{in}}} \times P_{\text{rated}} & ; v_{\text{in}} \leq v_a < v_{\text{rated}} \\ P_{\text{rated}} & ; v_{\text{rated}} \leq v_a < v_{\text{out}} \\ 0 & ; v_a \geq v_{\text{out}} \end{cases} \tag{28}$$

The PV output is calculated according to module Type D in [50], and shown by (29)–(33). G is the solar irradiance in $W/m_2$. The natural operating temperature *NOT* is 43°C, short-circuit current $I_{\text{SC}}$ and the open-circuit voltage $V_{\text{OC}}$ are 5.32 A and 21.98 V, respectively. Current $K_{\text{I}}$ and voltage $K_{\text{V}}$ coefficients are 1.22 A/°C and 14.4 mV/°C. The maximum current $I_{\text{MPP}}$ and maximum voltage $V_{\text{MPP}}$ are 4.76 A and 17.32 V. Each time interval data set, excluding the night-time intervals, is divided into 10 states. Then the probability of each state is calculated from the UCV PDF and the corresponding power of the state is calculated from:

$$T_{\text{c,s}} = T_{\text{a}} + \frac{\text{NOT} - 20°}{800} \cdot G \tag{29}$$

$$I_{\text{s}} = (I_{\text{SC}} + K_{\text{I}} \cdot (T_{\text{c,s}} - 25°)) \cdot \frac{G}{1000} \tag{30}$$

$$V_{\text{S}} = V_{\text{OC}} - K_{\text{V}} \times T_{\text{c,s}} \tag{31}$$

$$FF = \frac{V_{\text{MPP}} \cdot I_{\text{MPP}}}{V_{\text{OC}} \cdot I_{\text{SC}}} \tag{32}$$

$$P_{\text{PV}} = V_{\text{s}} \cdot I_{\text{s}} \cdot FF \tag{33}$$

### B. Scenario Generation From a Multinomial Distribution

A recurrent neural network is trained in [51] to predict temperature and solar irradiance based only on the date of the year and the time of the day. After that, the trained network is used to generate random weather scenarios. The bootstrap sampling technique is used in [52] to generate random wind scenarios. This technique does not incorporate the temporal correlation of the variables, and hence, would not work for PV scenarios. Awad *et al.* [29] optimize BESS sizing for all permutations of wind × load scenarios independently, assuming the BESS starts full in all scenarios. For each month of the year, the hours of the day (i.e. 24 hours) are divided to eight epochs of three hours each in [19],
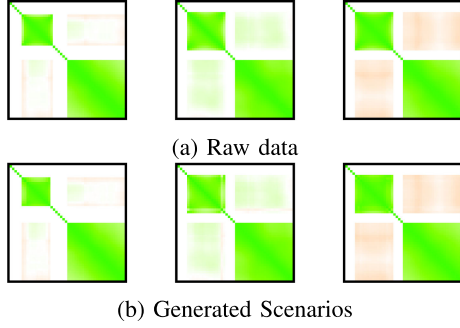
(a) Raw data



(b) Generated Scenarios

Fig. 3. Correlations among $\{G_{\text{PV}}(t), v_{\text{WT}}(t)\}$ of different hours of the day for a) Winter, b) Summer, c) Spring/fall.

and a markov-chain is trained to model wind-speed variations within each epoch. However, the markov-chains of different epochs are completely independent, and trained separately. The approaches of [19], [29], [52] destroy the diurnal patterns of data, and assume mutual independence of RES output between time periods. In order to be able to use any forecasting method in the hourly economic dispatch problem, the generated weather scenarios must incorporate the correlation in weather conditions among hours of the day.

Fig. 3(a) depicts a heat map for each of the three seasons, as follows: the color of each pixel represents the correlation factor between two of the 48 variables in the raw data. Variables 1–24 are the solar irradiances for hours 1–24. Variables 25-48 are the wind speeds for hours 1–24 as well. The top left quadrant depicts correlations among solar irradiances of different hours of the day. The bottom right quadrant represents correlations among wind speeds of different hours of the day. The top-right quadrant is a transposed copy of the bottom-left quadrant, and describe correlations between solar irradiances and wind speeds. Green color, red color, and white color indicate positive correlation, negative correlation, and no correlation, respectively. Darker areas indicate a stronger positive or stronger negative correlation, respectively. Solar irradiance is zero at night, and correlations cannot be calculated for these hours. Therefore, white color is used as an exception. For all 3 seasons, strong positive correlation exists among the solar irradiance of different hours within the day, and also among wind speeds of different hours within the day. Mild positive correlation exists between solar irradiance and wind speeds in Summer. Mild negative correlation exists between solar irradiance and wind speed in the Spring/Fall season. These observations prove that the proper approach to generate weather scenarios is by sampling from a multivariate distribution with correlation.

Vine copulas can be employed for this purpose [53], [54]. However, vine copulas require evaluating the conditional probability of each pair of variables in a multivariate distribution. In this paper, the solar irradiances and wind speeds for 24 hours make up 48 variables, giving rise to $(48!)/(2! \times 46!) = 1128$ pairs. Alternatively, It is possible to employ a Gaussian copula to generate random numbers and map each point to another desirable distribution [55]. This mapping is possible since the inverse cumulative density function (CDF) of the target distribution

can be evaluated, which is true for the multinomial distribution model discussed earlier.

Consider a multivariate probability distribution model $\mathcal{K}$ whose PDF is denoted as $k(X)$, CDF is denoted as $K(X)$, mean vector is denoted $\mu_k \in \mathbb{R}^m$, correlation matrix is denoted $\Sigma_k \in \mathbb{R}^{m \times m}$, and each event $X = (x_1, \ldots, x_m)$ consists of $m$ variables. The steps to generate a set $\mathbb{K}$ containing $|\mathbb{K}|$ instances, and matching the distribution $\mathcal{K}$, are as follows:

1) Generate a population $\mathbb{N}$ using a Gaussian number generator. The population $\mathbb{N}$ consists of $|\mathbb{N}| = |\mathbb{K}|$ instances, and each instance $X \in \mathbb{N}$ consists of $m$ variables (i.e. elements).
   - The value of $\boldsymbol{\mu}$ has no effect on the final population $\mathbb{K}$ because $\mathbb{N}$ is a proxy which will be mapped later to $\mathbb{K}$. $\boldsymbol{\mu} = \mathbf{0} = [0, \ldots, 0]^T$ can be used.
   - The correlation matrix $\boldsymbol{\Sigma_k}$ is fed to the Gaussian random number generator. In the special case that the variables are not correlated, $\boldsymbol{\Sigma_k}$ reduces to an identity matrix.

The generated population $\mathbb{N}$ is defined by (34). $\mathcal{N}$ denotes the normal (Gaussian) distribution. $\mathbb{N}$ has a PDF denoted $n(x)$, and a CDF denoted $N(X)$.

$$\mathbb{N} \sim \mathcal{N}(\mathbf{0}, \Sigma_k) \qquad (34)$$

2) For each instance $X \in \mathbb{N}$, calculate the CDF $N(X)$, incorporating $\boldsymbol{\mu}$ and $\boldsymbol{\Sigma_k}$. The CDF is defined as (35) and calculated as (36).

$$N(x_1, \ldots, x_n) = P[X_1 \leq x_1, \ldots, X_N \leq x_n] \qquad (35)$$

$$= \int_{-\infty}^{x_1} \ldots \int_{-\infty}^{x_m} n(x_1, \ldots, x_m) \, dx_1 \ldots dx_m \qquad (36)$$

3) Using the inverse-CDF $K^{-1}(p)$ of the target distribution $\mathcal{K}$, calculate the values of the random numbers. The inverse CDF is calculated as (37)

$$K^{-1}(p) = \min_{\mathbf{X}} \{\mathbf{X} : K(X) \geq p\} \qquad (37)$$

In short, a Gaussian random number generator is employed to generate a multi-variate population which has the desired covariance matrix. This population is, then, mapped to the target distribution. This method is commonly known as the *Sampling by inverse-transform*.

The KDE model used to fit the RES data is a multinomial distribution model. Weather scenarios are generated as explained, and the correlations among the variables in the generated scenarios are depicted in Fig. 3(b). The mild discrepancy between the two figures is loss of information caused by discretization of the data. The raw data of Fig. 3(a) has continuous values, while the generated scenarios are sampled from multinomial distributions.

## IV. ENHANCED RES FORECASTING

### A. An Ensemble of Deep Neural Networks

Deep neural networks can model complex phenomena by learning intricate patterns of large datasets. Recurrent neural networks (RNN) are particularly useful for modeling long-term
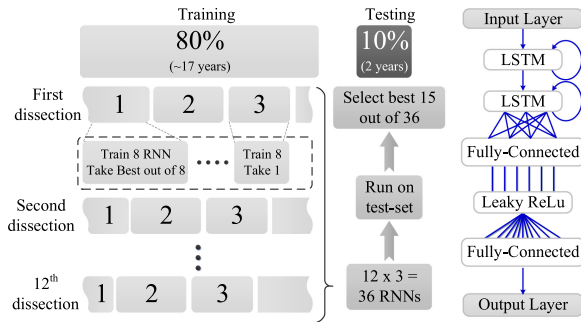
Fig. 4.   RNN architecture.

TABLE I
CASE STUDY PARAMETERS

| Param | Description | Value | Unit | Ref |
|---|---|---|---|---|
| $\overline{yr}$ | Project Lifetime | 25 | years | |
| $S$ | Salvage rate | 20 | %/year | |
| $F$ | Inflation rate | 1 | %/year | [29] |
| $IR$ | Interest rate | 5 | %/year | [29] |
| $\text{OvF}_{\text{PV}}$ | PV annual degradation | 0.95 | %/year | [58, 60] |
| $\eta_{\text{BESS}}$ | BESS round trip effic. | 90 | % | [44] |
| $SoC_{\min}$ | BESS min SoC | 0 | % | |
| $SoC_{\max}$ | BESS max SoC | 100 | % | |
| $\varphi$ | Fixed reserve margin | 0 | MW | |
| $\zeta$ | Future Uncertainty factor | 75 | % | |
| $\pi_{\text{BESS}}$ | BESS unit price | 550 | $/KWh | [44] |
| $\pi_{\text{Inv}}$ | BESS Inverter price | 100 | $/KW | [51] |
| $\pi_{\text{PV}}$ | PV cell unit price | 1,470 | $/KW | [58] |
| $\pi_{\text{WT}}$ | WT cell unit price | 1,600 | $/KW | [61] |

autocorrelated data for applications such as time-series fore-casting, natural language processing, and speech recognition. A variant of RNN called Long-Short-Term Memory (LSTM) networks is used in this paper to forecast weather parameters for the next 4 hours based on the weather data of the past 4 hours. The same raw dataset acquired from [45] and processed in Subsection III-A is used to train the neural networks. The raw data is split into training and testing sets on which 36 RNNs are trained. Out of 36 trained networks, the best 15 are extracted for use in the case study. The RNN architecture used in all networks is shown in Fig. 4.

### B. Multiplicative Weights Update (MWU)

Consider a set $\mathbb{I}$ of experts who provide technical advice to a decision maker at every interval (i.e. 1 hour) in an ongoing process (i.e. for 1 season). The advice of different experts must be analyzed and processed into a single decision. The final decision can be the advice of one of the experts selected with a probability, or the weighted sum of all expert's advices. It is intuitive to keep record of the benefit and harm $\chi$ brought by each expert over time. Eventually, experts who give better advice gain more credibility $\gamma_i$, and have a bigger influence on the final decision, such as higher probability of being selected in a draw, or a bigger weight towards the weighted sum. Littlestone *et al.* [56] propose a technique for updating the credibility scores $\gamma_i$ such that after a number of iterations, the decision maker ends up performing at least as good as what the best single expert alone would. This method is employed by [57] in a matrix-game for long-term investment planning in a power system, considering multiple climate scenarios. To the best of the authors' knowledge, this method has not been used for power system economic dispatch.

In this paper, each neural network represents an expert $i$ whose technical advice is a forecast of the wind-speeds and solar irradiances for the next 4 hours. The weighted average of the forecasts is used as the basis for the economic dispatch problem. The advantages of using the MWU in power system economic dispatch (ED) are as follows: different forecast algorithms and models can be used to produce forecasts, and an economic dispatch (ED) problem with a single weighted-average scenario is solved instead of solving a stochastic ED problem with a set of scenarios. In order to evaluate the performance of $|\mathbb{I}|$ forecasts and update the score credit of $|\mathbb{I}|$ experts, a deterministic

economic dispatch problem is solved independently for each expert's forecast. This can be done offline between dispatch periods, and in parallel on separate computing hardware with mediocre computational power.

The MWU formula is shown in [38]. $\chi_i$ is the cumulative profit brought by expert $i$ from the start $t = 1$ up to the current iteration $t$. $\gamma_i$ is the credibility score of expert $i$, which is also used as the weight of each forecast towards the final sum. $\sigma$ is called the "width parameter," and is used to scale down the numerator. $\sigma$ is usually assigned the largest profit theoretically possible. In this paper, $\sigma$ is set to be the revenue from selling the full HREP's capacity $C_{\text{HREP}}$ for the operation horizon $t + \{0, .., 4\}$. parameter $\varepsilon$ is a hyper-parameter which is used to tune the step-size of the update. With larger values, the algorithm takes bigger steps, approaches its terminal values faster, however, at the cost of worse performance (i.e. advice). At small values of $\varepsilon$, the algorithm converges slower while demonstrating better performance at the end of operation. It is worth mentioning that values of $\varepsilon \gg 1$ may lead $\gamma$ to grow to infinity, causing computational failure. %The parameter was tuned by trial and error, and a value of $\varepsilon = 0.1$ is adopted. After calculating $\gamma_i$ for all experts, the weights $\gamma_i$ are normalized by (39).

$$\gamma_i = \exp\left(-\varepsilon \frac{\chi_i}{2 \cdot \sigma}\right) \tag{38}$$

$$\check{\gamma}_i = \frac{\gamma_i}{\sum^i \gamma_i} \tag{39}$$

### V. PROPOSED CASE STUDY

The case parameters are listed in Table I. The electricity price $\pi_E^t$ profile consists of three levels. The average electricity price $137.5/MWh applies for the period [3:00-11:59], and the period [15:00-23:59] of every day. The price falls to $104.5/MWh in the period [00:00-02:59], and also rises to $187/MWh in the period [12:00-14:59]. This profile aligns with the average electricity price of $133/MWh in USA [58], and lies below the average price in France of $200/MWh [59].

Random scenarios consisting of 2184 hours are generated for each of the three seasons {Winter, Summer, Spring/Fall} using the scenario generation technique in subsection III-B. A total of

TABLE II
RAMPING POLICIES (RP) UNDER TESTING

| RP | $\alpha$ | $\beta$ | $A_{\tilde{\rho}}$ | $\tilde{\rho}_{\min}$ | RP | $\alpha$ | $\beta$ | $A_{\tilde{\rho}}$ | $\tilde{\rho}_{\min}$ |
|----|------|------|------|------|----|-------|------|------|------|
| 1 | -0.1 | 0.25 | 0.4 | 0.15 | 4 | -0.05 | 0.15 | 0.25 | 0.1 |
| 2 | 0 | 0.15 | 0.3 | 0.15 | 5 | -0.1 | 0.15 | 0.2 | 0.05 |
| 3 | -0.2 | 0.25 | 0.3 | 0.05 | 6 | -0.05 | 0.1 | 0.15 | 0.05 |

93 weather scenarios are generated. Costs and revenues of the Spring/Fall season are counted twice towards the total objective function. All tests are run on the same set of generated scenarios to ensure objective comparison. Each of the 93 weather scenarios are passed through the 15 trained RNNs (hour by hour) to obtain a four-hours ahead forecast at each hour. We explore solving the HREP design problem with and without a reserve margin of $\lambda = 5\%$ of available RES power, for 2 penalty levels on excessive ramping $\{\{200\%, 500\%\} \times \max^t\{\pi_E^t\}\}$. The penalty factor on deviation from the HA schedule is set as 25% of the penalty on excess ramping as well. Finally, we also explore 6 different policies $(\alpha, \beta)$ for the ramping limit. Therefore, 24 design scenarios are explored: 2 penalty factors $\times$ 2 reserve policies $\times$ 6 ramping policies.

A ramping policy $\alpha = 0.15$, $\beta = 0.05$ restrains ramping at low power output $P_{\mathrm{HREP}}$, but grants the HREP bigger ramping room at higher output level $P_{\mathrm{HREP}}$. Preliminary tests reveal that this RP leads to undesirable patterns in the HREP hourly dispatch schedule. When the penalty factor $\pi_{\hat{\rho}}$ is relatively low $< 150\% \times \max_t\{\pi_E^t\}$, the HREP has to choose between curtailing large amounts of RES or commit a strategic violation of the ramp-up limit to rise from low power level. This is for the purpose of reaching a high power output around hours with high-electricity price, when such hours befall within the forecast horizon. Therefore, the financial profit from selling electricity at a higher price justifies paying the penalty on excess ramping.

For high penalty factors above $> 400\% \times \max_t\{\pi_E^t\}$, significant amounts of renewable energy are abandoned in order to abide by the ramping limit and avoid the penalty. In fact, the average amount of spilled RE across all seasons exceeds 25% of the total available RE. Therefore, this policy is deemed counterproductive, which can also be foreshadowed for all policies with $\alpha > 0$. Based on this observation, the case-study focuses on policies with $\alpha \leq 0$, and $\beta \geq 0.05$. The ramping policies considered in this paper are listed in Table II. This table also reports the total area of the permissible ramping bandwidth $A_{\tilde{\rho}} = \alpha + 2\beta$, and the smallest ramping room: $\min\{\tilde{\rho}\} = \alpha + \beta$ in the band. $\min\{\tilde{\rho}\}$ occurs at the maximum power output $P_{\mathrm{HREP}} = 100\%$.

The hourly dispatch problem is formulated in MATLAB using MATPOWER's optimum scheduling tool (MOST) [62]. The linear-program solver from the CPLEX suite is used for the hourly economic dispatch problem. A dedicated model is developed separately for the optimal sizing and design problem. As mentioned earlier, the RFC algorithm cannot be represented in closed form. At the same time, the proxy value $\pi_{P_{\mathrm{BESS}}}$ has an indirect effect on the BESS lifelong degradation, and therefore, $\pi_{P_{\mathrm{BESS}}}$ can only be optimized heuristically. The Genetic Algorithm is employed to solve this black-box problem. Evaluation of a



(a) Main Process
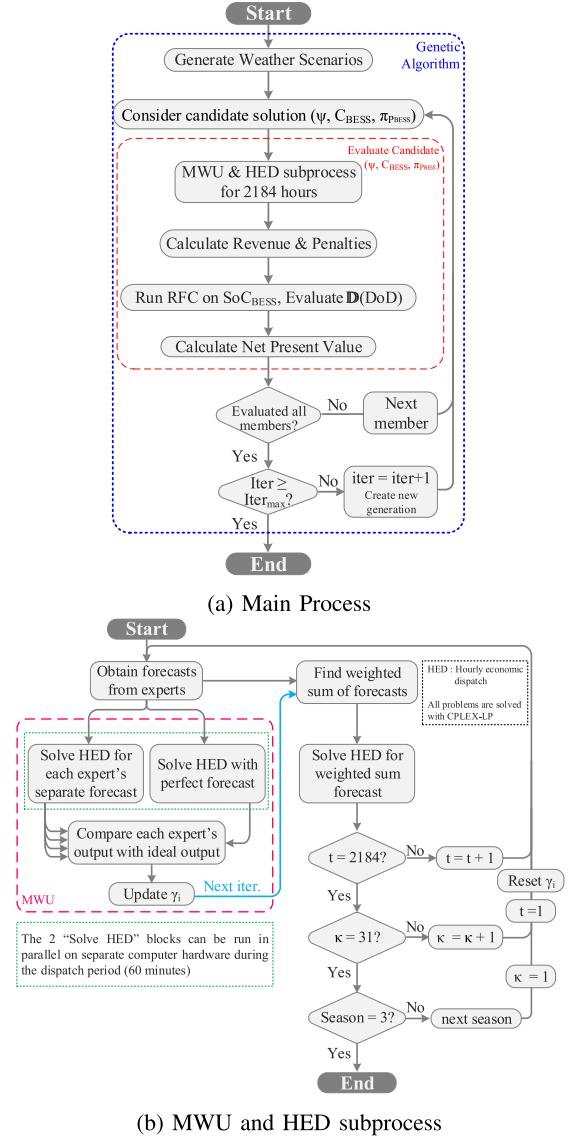


(b) MWU and HED subprocess

Fig. 5. Optimization of HREP design and operation.

single candidate solution involves running the hourly dispatch scheduling problem $\{31 \text{ scenarios}\} \times \{3 \text{ seasons}\} \times \{2184 \text{ periods}\}$, and also running the RFC algorithm to process the BESS profile. The final stage of evaluating a candidate solution is running a peripheral process to determine the oversizing factor of the BESS. The simulations are run on a high-performance computing cluster with 24 dedicated cores. Evaluation of a single candidate solution requires 10 minutes on this hardware setup. The whole optimization process requires between 48-72 hours. The full problem formulation is described by the flowchart in Fig. 5. Eqs. (40)–(42) illustrate the bounds of the decision variables of the design problem.

$$10\% \leq \psi \qquad\qquad \leq 90\% \qquad\qquad (40)$$

$$0.1\% \leq C_{\mathrm{BESS}} \qquad\qquad \leq 50\% \qquad\qquad (41)$$

$$0 \leq \pi P_{\mathrm{BESS}} \qquad\qquad \leq 500\% \cdot \max_t\{\pi_E^t\} \qquad (42)$$

TABLE III
MAIN RESULTS $\{\psi, C_{\text{BESS}}, \pi_{P_{\text{BESS}}}, OvF_{\text{BESS}}, \text{PROFIT}, P_{\text{CURT}}\}$

| RP | $\psi$ (%) | $C_{\text{BESS}}$ (%) | $\pi_{P_{\text{BESS}}}$ (%) | $OvF_{\text{BESS}}$ (%) | Profit (M$) | $P_{\text{curt}}$ (%) | $\psi$ (%) | $C_{\text{BESS}}$ (%) | $\pi_{P_{\text{BESS}}}$ (%) | $OvF_{\text{BESS}}$ (%) | Profit (M$) | $P_{\text{curt}}$ (%) |
|---|---|---|---|---|---|---|---|---|---|---|---|---|
| | $\pi_{\hat{\rho}} = 200\%$, $\lambda = 0\%$ | | | | | | $\pi_{\hat{\rho}} = 200\%$, $\lambda = 5\%$ | | | | | |
| 1 | 10.6 | 41.4 | 81.1 | 6.1 | 266 | 1.2 | 12.2 | 27.9 | 50.2 | 7.8 | 248.4 | 6 |
| 2 | 13.3 | 36.6 | 100.2 | 6.6 | 263.5 | 2.9 | 12.6 | 28.1 | 100.4 | 7.6 | 244.3 | 7.6 |
| 3 | 20.3 | 16 | 58.5 | 10.3 | 252 | 1.4 | 16.3 | 16.2 | 58 | 10.3 | 233.7 | 6.3 |
| 4 | 20.8 | 12.9 | 81.4 | 11.1 | 249.1 | 2.6 | 16.5 | 11.6 | 89.8 | 12.8 | 229.9 | 7.5 |
| 5 | 24.2 | 10.6 | 105.6 | 11.3 | 240.3 | 2.9 | 20.9 | 11.3 | 94.3 | 11.5 | 222.5 | 7.7 |
| 6 | 24.9 | 8.9 | 94.7 | 12.6 | 226 | 4.6 | 22.4 | 12.4 | 97.4 | 10.8 | 210.4 | 9.1 |
| | $\pi_{\hat{\rho}} = 500\%$, $\lambda = 0\%$ | | | | | | $\pi_{\hat{\rho}} = 500\%$, $\lambda = 5\%$ | | | | | |
| 1 | 31.2 | 50 | 110.6 | 5.6 | 200.5 | 5.9 | 28.3 | 50 | 110.7 | 5.3 | 187.3 | 10.3 |
| 2 | 30.1 | 50 | 125.7 | 5.1 | 210.6 | 6.4 | 30 | 50 | 125.9 | 5 | 194.7 | 10.9 |
| 3 | 39.8 | 12.9 | 84.8 | 11.4 | 166.2 | 10.3 | 37.1 | 25.3 | 139.1 | 7.5 | 156.5 | 12.1 |
| 4 | 30.4 | 50 | 140.4 | 4.7 | 170.4 | 7 | 29.3 | 50 | 140.9 | 4.8 | 157.2 | 11.5 |
| 5 | 37.1 | 8.9 | 116.6 | 12.1 | 137.2 | 11.8 | 34.2 | 12.9 | 95.9 | 10.9 | 128.1 | 15 |
| 6 | 34.1 | 49.9 | 134.7 | 4.2 | 143.2 | 9.1 | 34.9 | 49.9 | 134.5 | 4.2 | 132.8 | 12.9 |

TABLE IV
STATISTICS OF $\{\hat{\rho}^{\pm}, \delta^{\pm}\}$

| RP | $\pi_{\hat{\rho}}$ | $\lambda$ | $\hat{\rho}^{-,t}$ # | $\sum^t(\cdot)$ | $\hat{\rho}^{+,t}$ # | $\sum^t(\cdot)$ | $\delta^{-,t}$ # | $\sum^t(\cdot)$ | $\delta^{+,t}$ # | $\sum^t(\cdot)$ |
|---|---|---|---|---|---|---|---|---|---|---|
| 1 | 200 | 0 | 61.1 | 627.3 | - | - | 639.5 | 4,631 | 337.2 | 3,769 |
| 2 | 200 | 0 | 83.6 | 680 | 4.8 | 28.1 | 346.7 | 3,499 | 336.3 | 3,208 |
| 3 | 200 | 0 | 80.7 | 870.5 | - | - | 723.7 | 5,561 | 532.3 | 5,133 |
| 4 | 200 | 0 | 93.3 | 872 | 6.5 | 45.4 | 764.5 | 5,607 | 585 | 4,856 |
| 5 | 200 | 0 | 114.4 | 1,037 | 5.5 | 30.4 | 742.1 | 5,781 | 634 | 5,104 |
| 6 | 200 | 0 | 163.4 | 1,242 | 23.5 | 206.2 | 785.5 | 5,735 | 703 | 4,719 |
| 1 | 200 | 5 | 56.3 | 525.3 | - | - | 663.4 | 4,794 | 354.9 | 3,823 |
| 2 | 200 | 5 | 84.6 | 678.1 | 3.1 | 13.5 | 415.2 | 3,802 | 354.2 | 3,246 |
| 3 | 200 | 5 | 77.5 | 849 | - | - | 700.8 | 5,301 | 519.6 | 4,986 |
| 4 | 200 | 5 | 88.1 | 861.5 | 6.1 | 42.7 | 694.3 | 5,409 | 589.7 | 4,895 |
| 5 | 200 | 5 | 109.4 | 1,003 | 5.4 | 29.3 | 711.8 | 5,411 | 603.6 | 4,795 |
| 6 | 200 | 5 | 165.1 | 1,234 | 25 | 207.5 | 751.4 | 5,153 | 601.5 | 3,866 |
| 1 | 500 | 0 | 45.2 | 320.9 | - | - | 386 | 3,010 | 111.9 | 825 |
| 2 | 500 | 0 | 59.8 | 394.2 | - | - | 222.8 | 2,065 | 100.7 | 725.1 |
| 3 | 500 | 0 | 52.3 | 396.8 | - | - | 672.7 | 5,043 | 64.8 | 483.9 |
| 4 | 500 | 0 | 89.2 | 658.7 | 0.03 | 0.02 | 527.4 | 3,042 | 303 | 1,292 |
| 5 | 500 | 0 | 94.2 | 666.9 | - | - | 819 | 5,604 | 141.5 | 827.9 |
| 6 | 500 | 0 | 103.9 | 790.6 | 3.1 | 4.8 | 648.6 | 2,887 | 483.2 | 1,650 |
| 1 | 500 | 5 | 41.3 | 298.9 | - | - | 350.9 | 2,751 | 109.5 | 808.5 |
| 2 | 500 | 5 | 55.1 | 346.9 | - | - | 208.1 | 1,866 | 93.2 | 658.8 |
| 3 | 500 | 5 | 68.1 | 496.5 | - | - | 552.7 | 4,171 | 84.4 | 613.8 |
| 4 | 500 | 5 | 80.9 | 586.5 | 0.01 | 0.004 | 498.3 | 2,799 | 296 | 1,226 |
| 5 | 500 | 5 | 101.1 | 683.9 | - | - | 750.9 | 4,963 | 149 | 831 |
| 6 | 500 | 5 | 98.2 | 720.8 | 2 | 2.7 | 620.9 | 2,634 | 470.2 | 1,537 |

TABLE V
STATISTICS OF $\{\rho^{\pm}, \delta^{\pm}\}$

| RP | $\pi_{\hat{\rho}}$ | $\lambda$ | $\rho$ (MW/hr) min | $p_{0.5}$ | $p_{99.5}$ | max | $\delta$ (MW) min | $p_{0.5}$ | $p_{99.5}$ | max |
|---|---|---|---|---|---|---|---|---|---|---|
| 1 | 200 | 0 | -95.6 | -34.7 | 24.8 | 25 | -77.4 | -31.7 | 29.8 | 50 |
| 2 | 200 | 0 | -87.9 | -31.6 | 15 | 35.9 | -72.9 | -28.8 | 25.8 | 49.9 |
| 3 | 200 | 0 | -81.3 | -33.3 | 23.1 | 25 | -78.9 | -31.7 | 31 | 50 |
| 4 | 200 | 0 | -79.4 | -32.3 | 15 | 32.1 | -77.6 | -29.3 | 25.9 | 52.1 |
| 5 | 200 | 0 | -76 | -31.5 | 15 | 27 | -75.3 | -28.6 | 25.1 | 50 |
| 6 | 200 | 0 | -74.2 | -30.5 | 13.7 | 42.8 | -73.7 | -28.1 | 20 | 50.6 |
| 1 | 200 | 5 | -84.3 | -32.9 | 24.4 | 25 | -72.1 | -32.1 | 29.8 | 50 |
| 2 | 200 | 5 | -85.2 | -31.6 | 15 | 30.1 | -70.2 | -28.6 | 25.3 | 47 |
| 3 | 200 | 5 | -81 | -33.2 | 23.1 | 25 | -77.6 | -31.4 | 31 | 50 |
| 4 | 200 | 5 | -79.3 | -32.7 | 15 | 32.1 | -77.7 | -29.2 | 26.3 | 53.9 |
| 5 | 200 | 5 | -75.1 | -30.9 | 15 | 26.3 | -74.6 | -28 | 25 | 50.3 |
| 6 | 200 | 5 | -73.7 | -29.3 | 14.1 | 41.3 | -72.2 | -26.6 | 19.5 | 49.3 |
| 1 | 500 | 0 | -70.7 | -28 | 24.8 | 25 | -61.3 | -23.4 | 12.5 | 37.5 |
| 2 | 500 | 0 | -66.9 | -25.5 | 15 | 15 | -68.1 | -21.9 | 12.3 | 34.5 |
| 3 | 500 | 0 | -60.2 | -25.3 | 22.5 | 25 | -59.5 | -25.3 | 8.7 | 38.8 |
| 4 | 500 | 0 | -78.8 | -26.7 | 15 | 15.3 | -67.7 | -22.6 | 11.7 | 35.1 |
| 5 | 500 | 0 | -62.9 | -25.3 | 14.6 | 15 | -62.6 | -24.3 | 11.5 | 30 |
| 6 | 500 | 0 | -74 | -23.4 | 10 | 19 | -58.3 | -18.7 | 10 | 35.3 |
| 1 | 500 | 5 | -70.4 | -27.9 | 24.8 | 25 | -60.8 | -22.8 | 12.4 | 39.6 |
| 2 | 500 | 5 | -63.6 | -24.6 | 15 | 15 | -63.9 | -20.5 | 11.6 | 32.3 |
| 3 | 500 | 5 | -62.4 | -26.4 | 23.6 | 25 | -53.8 | -23.2 | 10.4 | 38.6 |
| 4 | 500 | 5 | -76.9 | -26 | 15 | 15.2 | -65.3 | -21.6 | 11 | 32.3 |
| 5 | 500 | 5 | -62.5 | -25 | 14.8 | 15 | -61.8 | -23.7 | 11.1 | 30 |
| 6 | 500 | 5 | -66.2 | -22.4 | 10 | 16.4 | -53.1 | -17.5 | 9.9 | 32.7 |

## VI. RESULTS AND DISCUSSION

### A. Results of All 24 Design Regulations

The optimum HREP design parameters: $\psi$, $C_{\text{BESS}}$, $\pi_{P_{\text{BESS}}}$, and $OvF_{\text{BESS}}$ are listed in Table III. It is observable that a higher penalty $\pi_{\hat{\rho}}$ always leads to a larger PV unit $\psi$, which implies that PV power is less volatile than wind power. Moreover, most of the design scenarios with a higher penalty $\pi_{\hat{\rho}}$ have a larger BESS unit $C_{\text{BESS}}$, and a smaller BESS oversizing factor $OvF_{\text{BESS}}$ compared to the results with low penalty $\pi_{\hat{\rho}}$. A higher penalty $\pi_{\hat{\rho}}$ also leads to a higher proxy value of BESS stored energy $\pi_{P_{\text{BESS}}}$. This indicates that flexibility becomes more important than utilizing the BESS in arbitrage, in light of the high penalty. Given the higher proxy price of BESS energy, the BESS is utilized less aggressively, and the BESS experiences smaller discharge cycles. Hence, the BESS suffers less degradation $\mathbb{D}_{\text{PV}}$, and the required $OvF_{\text{BESS}}$ is smaller.

Further analysis is conducted on violations of the ramping policy (RP) and the magnitudes of HA-deviation. Table IV provides a survey of RP violations $\hat{\rho}$ and deviation from HA schedule $\delta$. The number (#) and total magnitude ($\sum^t(\cdot)$) of both types of violation events are reported. It is noticeable that the reserve criterion $\lambda = 5\%$ reduces the number and total mangitude of ramping violations for most RPs. A higher penalty $\pi_{\hat{\rho}}$ is more effective at reducing all types of violations. The resreve criterion $\lambda = 5\%$ also reduces the number and total magnitude of hour-ahead deviations $\delta$ for most RPs.

Additional details about the operation aspects of each design are given in Table V. For each design, the actual ramping $\rho^t$ profiles of all seasons and all weather scenarios are consolidated for statistical analysis. The extreme values (min, max) are reported. The 0.5 and 99.5 percentiles $\{p_{0.5}, p_{99.5}\}$ are also reported since they exclude extremely rare events, which helps conducting a fair comparison between RPs. The same analysis is carried out for the deviation from HA schedule $\delta^t$. The lower half of Table IV shows that for all different RPs and different $\lambda$, when $\pi_{\hat{\rho}} = 500\%$, violations of the ramp-up limit are very rare. Table V confirms this statistic since the maximum ramp-up $\rho^+$ is close to the actual limit $\beta$ in each row. The 99.5 percentile is below the limit in few cases.

The system operator selects the RP based on the reserve available from existing units. Extreme ramping data indicate how much additional ramping reserve is required; while extreme HA-deviation $\delta$ data indicate how much additional power-capacity reserve is required. Table V shows that the magnitude of extreme ramp-down events is generally larger than the magnitude of down HA-deviation events, despite that HA deviations incur a smaller penalty. These findings align with the findings of [1]–[5]; that is, the primary effect of RES integration in the power

TABLE VI
COMPARISON: MWU VS. SIMPLE AVERAGE FORECAST

| RP | $\varepsilon$ | Objective (M$) | | Improvement | | $\varepsilon$ | Objective (M$) | | Improvement | |
|---|---|---|---|---|---|---|---|---|---|---|
| | | Avg | MWU | K$ | % | | Avg | MWU | K$ | % |
| | $\pi_{\hat{\rho}} = 200\%,\ \lambda = 0\%$ | | | | | $\pi_{\hat{\rho}} = 200\%,\ \lambda = 5\%$ | | | | |
| 1 | 0.049 | 265.5 | 266 | 471.6 | 0.178 | 0.061 | 247.6 | 248.4 | 753.2 | 0.304 |
| 2 | 0.07 | 263 | 263.5 | 497 | 0.189 | 0.067 | 243.9 | 244.3 | 381.1 | 0.156 |
| 3 | 0.052 | 251.5 | 252 | 542.7 | 0.216 | 0.052 | 233.3 | 233.7 | 437.8 | 0.188 |
| 4 | 0.073 | 248.5 | 249.1 | 538.3 | 0.217 | 0.067 | 229.5 | 229.9 | 439.3 | 0.191 |
| 5 | 0.076 | 239.3 | 240.3 | 994.2 | 0.416 | 0.07 | 222 | 222.5 | 525.2 | 0.237 |
| 6 | 0.099 | 225.2 | 226 | 874.4 | 0.388 | 0.079 | 209.2 | 210.4 | 1,131 | 0.541 |
| | $\pi_{\hat{\rho}} = 500\%,\ \lambda = 0\%$ | | | | | $\pi_{\hat{\rho}} = 500\%,\ \lambda = 5\%$ | | | | |
| 1 | 0.085 | 199.1 | 200.5 | 1,399 | 0.703 | 0.076 | 186.4 | 187.3 | 858 | 0.46 |
| 2 | 0.096 | 209 | 210.6 | 1,563 | 0.748 | 0.1 | 193.1 | 194.7 | 1,559 | 0.807 |
| 3 | 0.123 | 162.1 | 166.1 | 4,106 | 2.533 | 0.094 | 153.4 | 156.5 | 3,123 | 2.036 |
| 4 | 0.126 | 168.7 | 170.3 | 1,705 | 1.011 | 0.141 | 155.5 | 157.2 | 1,643 | 1.057 |
| 5 | 0.144 | 133.7 | 137 | 3,575 | 2.674 | 0.138 | 124.9 | 128.1 | 3,157 | 2.527 |
| 6 | 0.165 | 141 | 143 | 2,116 | 1.5 | 0.114 | 130.9 | 132.8 | 1,923 | 1.47 |

system is an increased requirement for load-following reserve (i.e. ramping reserve).

It can be noticed that the reserve criterion $\lambda = 5\%$ yields a small improvement on extreme ramping and HA-deviation. Moreover, later RPs may suppress the worst (i.e. extreme) ramping and HA-deviation events, however, small-magnitude violations occur much more often. With a low penalty $\pi_{\hat{\rho}}$, later RPs suppress extreme (i.e. min, max) ramping events. With a high penalty $\pi_{\hat{\rho}}$, a stringent RP exacerbates extreme ramping events. The HREP operator collects a higher overall profit with a low penalty factor $\pi_{\hat{\rho}}$ and with the first RPs. Hence, the system operator is advised to adopt a small penalty with RP 6, or a high penalty with RPs 2 or 3.

The design scenario with RP 3, high penalty $\pi_{\hat{\rho}} = 500\%$, and no reserve $\lambda = 0\%$ features the least severe worst-case-scenario of ramping-down ($\rho^- = -60.2$ MW/hr), one of the least severe worst-case scenarios of hour-ahead deviation ($\delta^- = 59.5$ MW), and a relatively small number (52.3) and total magnitude (396.8 MW/hr) of ramping-down violations per season. Therefore, this design scenario is recommended for implementation. Consequently, the optimum HREP design is {$\psi = 39.8\%$, $C_{\text{BESS}} = 12.9\%, \pi_{P_{\text{BESS}}} = 84.8\%$}. This corresponds to a HREP with a PV plant of capacity 39.8MW, a WT plant of capacity 60.2MW, a BESS unit with capacity 12.9 MWh. The proxy value of energy stored in the BESS is $84.8\% \times 187 = 158.6$\$/MWh. The penalty on violating the RP is $500\% \times 187 = \$935$/MW/hr. The penalty on deviation from the HA schedule is $25\% \times 935 = \$233.8$/MW. For this HREP design, a segment from the hourly dispatch profiles of a Summer scenario is shown in Fig. 6. The grey line represents the electricity price $\pi_E^t$, referred to the right axis. The remaining graphs are referred to the left axis.

From $t = 679$ to $t = 682$, the HREP is ramping up at the maximum rate. As the HREP's output $P_{\text{HREP}}^t$ rises, the permissible ramping envelope $\tilde{\rho}^t$ tightens since $\alpha < 0$ (i.e. $\alpha = -0.2$). The BESS is already fully charged at $t = 679$, and remains full. Therefore, the HREP spills some RE. A temporary rise in available RE is forecasted for $t = 727$, with a sharp drop
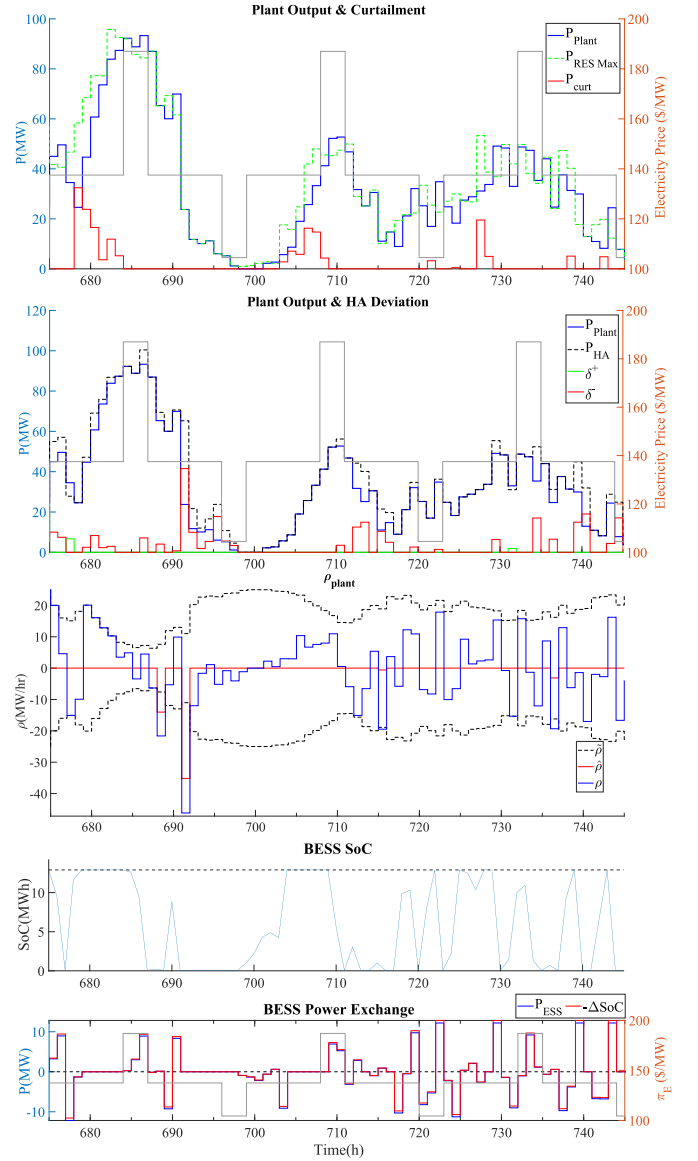


Fig. 6. Operation profile for a summer season for recommended HREP.

forecasted for the following hour. Therefore, the HREP does not export the full available RE at $t = 727$ in order to avoid a steep ramp-down on the following hour. The surplus RE is utilized to charge up the battery fully. The BESS profile reveals that the BESS avoids charging up during hours of high energy price. However, the BESS charges up at $t = 732$ despite the high price of electricity. This is because the actual available RE is higher than the HA commitment. Hence, the HREP abides by its HA commitment, and uses the surplus RE to charge up the fully depleted BESS.

### B. Analysis of All Weather Scenarios in Selected Design

The hourly dispatch profiles of all 31 scenarios and 3 seasons are consolidated, and represented by histogram plots in Figs. 7–9. The analysis involves: RES curtailment, RP violations, and deviations from HA schedule. For example, RES curtailment
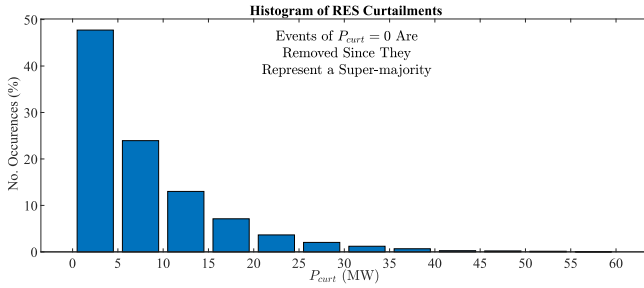
Fig. 7.    Histogram of $P_{\text{curt}}$ for recommended design.
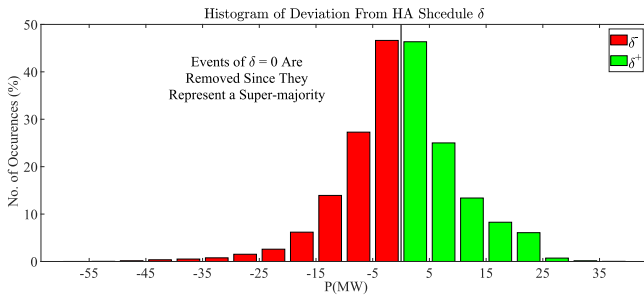


Fig. 8.    Histogram of $\delta$ for recommended design.
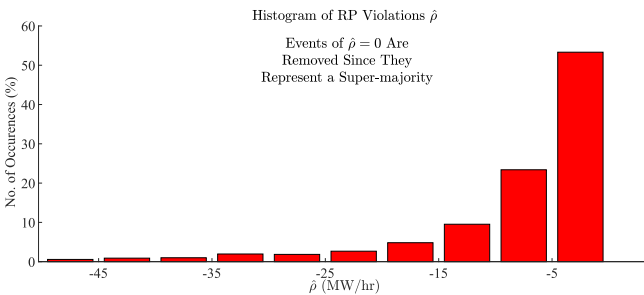


Fig. 9.    Histogram of $\hat{\rho}$ for recommended design.

events with similar magnitude are grouped together, and the number of occurrences in each group is reported. The proposed REMS framework demonstrates good performance such that events with $P_{\text{curt}} = 0$MW are the most frequent among all events of $P_{\text{curt}}$. Therefore, cases of $P_{\text{curt}} = 0$MW are excluded from the histogram plots. Similarly, events of $\hat{\rho} = 0$, and $\delta = 0$ represent a super-majority in their population, and therefore, are not shown in the histogram plots. Small RE curtailment events of magnitude up to 5MW represent 47.7% of all non-zero curtailment events.

Figs. 8 and 9 elaborate over the information given in Table V for the specific HREP design: RP 3, high $\pi_{\hat{\rho}}$, $\lambda = 0\%$, $\{\psi = 39.8\%, C_{\text{BESS}} = 12.9\%, \pi_{P_{\text{BESS}}} = 84.8\%\}$. It can be noticed that the largest violations and deviations are extremely rare events. While the worst ramping-down event is $-60.2$MW/hr, 99% of all RP violations ($\pm$) fall between $-25.3$MW/hr and $+22.5$MW/hr (i.e. no violations of ramp-up limit). Similarly, the worst HA deviation event is $-59.5$MW, but 99% of HA deviation events fall between $-25.3$MW and 8.7MW.

## C. Added Value of Multiplicative Weights Update

Table VI demonstrates the advantage of using the MWU algorithm for forecasting over taking the simple average forecast. The MWU algorithm helps acquiring better forecasts. Consequently, the system commits fewer violations, and bears less penalties. The advantage of the MWU algorithm is most apparent when a high penalty is applied $\pi_{\hat{\rho}} = 500\%$. In the case of recommended design (i.e. RP 3, high $\pi_{\hat{\rho}} = 500\%$, no reserve $\lambda = 0\%$), the MWU contributes a 2.533% cost improvement over taking the simple average of all forecasts.

## VII. CONCLUSION

This paper develops a comprehensive framework for optimum design and operation of a hybrid renewable energy plant (HREP). The advantages of the proposed framework over existing frameworks are: improved forecasting technique, suppressing extreme inter-hour ramping to mitigate the volatility aspect of RES, suppressing deviation from the HA dispatch plan to mitigate the uncertainty aspect of RES, and finally, the use of a proxy variable for the value of energy stored in battery storage to optimize engagement in arbitrage versus provision of flexibility. Improved forecasts are obtained through deep-learning, and the novel use of the multiplicative weights update method. The output of the hourly economic dispatch problem is used to optimize the HREP design. The proposed operation philosophy yields a low total RES curtailment level between 1.2% and 15%, depending on operation limits. 99% of all ramping events fall within the defined ramping limits. In light of the findings of this design, regulators of the electricity sector are recommended to specify limits on the ramping rate of RES at the 30-minutes and 1-hour time-frames, conduct cost/benefit analysis for careful tuning of the penalty factor on violating these ramping limits, and adopting a dynamic ramping limit.

## REFERENCES

[1] B. Mohandes, M. S. E. Moursi, N. Hatziargyriou, and S. El-Khatib, "A review of power system flexibility with high penetration of renewables," *IEEE Trans. Power Syst.*, vol. 34, no. 4, pp. 3140–3155, Jul. 2019.

[2] M. Huber, D. Dimkova, and T. Hamacher, "Integration of wind and solar power in Europe: Assessment," *Energy*, vol. 69, pp. 236–246, 2014.

[3] M. A. Matos and R. J. Bessa, "Setting the operating reserve using probabilistic wind power forecasts," *IEEE Trans. Power Syst.*, vol. 26, no. 2, pp. 594–603, May 2011.

[4] H. Holttinen *et al.*, "Methodologies to determine operating reserves due to increased wind power," *IEEE Trans. Sustain. Energy*, vol. 3, no. 4, pp. 713–723, Oct. 2012.

[5] S. Veda *et al.*, "Evaluating the impact of the 2017 solar eclipse on U.S. western interconnection operations," Apr. 2018, doi: 10.2172/1435500.

[6] P. Sørensen *et al.*, "Power fluctuations from large wind farms," *IEEE Trans. Power Syst.*, vol. 22, no. 3, pp. 958–965, Aug. 2007.

[7] S. S. Reddy and J. A. Momoh, "Realistic and transparent optimum scheduling strategy for hybrid power system," *IEEE Trans. Smart Grid*, vol. 6, no. 6, pp. 3114–3125, Nov. 2015.

[8] A. K. Barnes, J. C. Balda, and A. Escobar-Mejía, "A semi-markov model for control of energy storage in utility grids and microgrids with PV generation," *IEEE Trans. Sustain. Energy*, vol. 6, no. 2, pp. 546–556, Apr. 2015.

[9] Enirgenet, "Technical regulation 3.2.2 for wind power plants above 11 kW," Tech. Rep. 13/96336-43, Jun. 2016. [Online]. Available: https://en.energinet.dk/Electricity/Rules-and-Regulations/Regulations-for-grid-connection

[10] National Grid Electricity Transmission, "The [GB] grid code," Sustain. Energy Authority Ireland, Tech. Rep., no. 5, Dec. 2020. [Online]. Available: https://www.nationalgrid.com/sites/default/files/documents/8589935310-Complete%20Grid%20Code.pdf

[11] EirGrid, "EirGrid grid code," Tech. Rep., Jun. 2019. [Online]. Available: http://www.eirgridgroup.com/site-files/library/EirGrid/Grid-Code.pdf

[12] Dansk Energi, "Sustainable energy authority of Ireland SEAI," Sustain. Energy Authority reland, Tech. Rep., Jan. 2019. [Online]. Available: https://www.seai.ie/publications/Renewable-Energy-in-Ireland-2019.pdf

[13] D. Lee, J. Kim, and R. Baldick, "Stochastic optimal control of the storage system to limit ramp rates of wind power output," *IEEE Trans. Smart Grid*, vol. 4, no. 4, pp. 2256–2265, Dec. 2013.

[14] C. M. Correa-Posada, G. Morales-España, P. Dueñas, and P. Sánchez-Martín, "Dynamic ramping model including intraperiod ramp-rate changes in unit commitment," *IEEE Trans. Sustain. Energy*, vol. 8, no. 1, pp. 43–50, Jan. 2017.

[15] G. Morales-España, A. Ramos, and J. García-González, "An MIP formulation for joint market-clearing of energy and reserves based on ramp scheduling," *IEEE Trans. Power Syst.*, vol. 29, no. 1, pp. 476–488, Jan. 2014.

[16] E. A. Bakirtzis, P. N. Biskas, and A. G. Bakirtzis, "The impact of load-following reserve requirement levels on the short-term generation scheduling," in *Proc. Power Syst. Comput. Conf.*, 2016, pp. 1–7.

[17] E. Saiz-Marin, J. Garcia-Gonzalez, J. Barquin, and E. Lobato, "Economic assessment of the participation of wind generation in the secondary regulation market," *IEEE Trans. Power Syst.*, vol. 27, no. 2, pp. 866–874, May 2012.

[18] Y. Wang, H. Bayem, M. Giralt-Devant, V. Silva, X. Guillaud, and B. Francois, "Methods for assessing available wind primary power reserve," *IEEE Trans. Sustain. Energy*, vol. 6, no. 1, pp. 272–280, Jan. 2015.

[19] M. Hedayati-Mehdiabadi, K. W. Hedman, and J. Zhang, "Reserve policy optimization for scheduling wind energy and reserve," *IEEE Trans. Power Syst.*, vol. 33, no. 1, pp. 19–31, Jan. 2018.

[20] B. Hoseinali, R. Mario, and V. Daniel, "Optimization-based power management of a wind farm with battery storage," *Wind Energy*, vol. 16, no. 8, pp. 1197–1211, 2012. [Online]. Available: https://onlinelibrary.wiley.com/doi/abs/10.1002/we.1547

[21] A. Olama, P. R. C. Mendes, and E. F. Camacho, "Lyapunov-based hybrid model predictive control for energy management of microgrids," *IET Gener. Transmiss. Distrib.*, vol. 12, no. 21, pp. 5770–5780, 2018.

[22] A. Khatamianfar, M. Khalid, A. V. Savkin, and V. G. Agelidis, "Improving wind farm dispatch in the australian electricity market with battery energy storage using model predictive control," *IEEE Trans. Sustain. Energy*, vol. 4, no. 3, pp. 745–755, Jul. 2013.

[23] J. Martins, S. Spataru, D. Sera, D.-I. Stroe, and A. Lashab, "Comparative study of ramp-rate control algorithms for PV with energy storage systems," *Energies*, vol. 12, no. 7, pp. 1–15, 2019. [Online]. Available: https://www.mdpi.com/1996-1073/12/7/1342

[24] D. Lee, J. Kim, and R. Baldick, "Limiting ramp rate of wind power output using a battery based on the variance gamma process," in *Proc. Int. Conf. Renewable Energies Power Qual.*, 2012, pp. 1–5.

[25] X. Li, D. Hui, and X. Lai, "Battery energy storage station (BESS)-based smoothing control of photovoltaic (PV) and wind power generation fluctuations," *IEEE Trans. Sustain. Energy*, vol. 4, no. 2, pp. 464–473, Apr. 2013.

[26] H. Farzin, M. Fotuhi-Firuzabad, and M. Moeini-Aghtaie, "A stochastic multi-objective framework for optimal scheduling of energy storage systems in microgrids," *IEEE Trans. Smart Grid*, vol. 8, no. 1, pp. 117–127, Jan. 2017.

[27] C. Chen, S. Duan, T. Cai, B. Liu, and G. Hu, "Smart energy management system for optimal microgrid economic operation," *IET Renewable Power Gener.*, vol. 5, no. 3, pp. 258–267, 2011.

[28] T. A. Nguyen and M. L. Crow, "Stochastic optimization of renewable-based microgrid operation incorporating battery operating cost," *IEEE Trans. Power Syst.*, vol. 31, no. 3, pp. 2289–2296, May 2016.

[29] A. Awad, T. EL-Fouly, and M. Salama, "Optimal ESS allocation for benefit maximization in distribution networks," *IEEE Trans. Smart Grid*, vol. 8, no. 4, pp. 1668–1678, Jul. 2017.

[30] D. Tran and A. M. Khambadkone, "Energy management for lifetime extension of energy storage system in micro-grid applications," *IEEE Trans. Smart Grid*, vol. 4, no. 3, pp. 1289–1296, Sep. 2013.

[31] V. Muenzel, J. Hoog, M. Brazil, A. Vishwanath, and S. Kalyanaraman, "A multi-factor battery cycle life prediction methodology for optimal battery management," in *Proc. ACM 6th Int. Conf. Future Energy Syst.*, 2015, pp. 57–66.

[32] K. Abdulla *et al.*, "Optimal operation of energy storage systems considering forecasts and battery degradation," *IEEE Trans. Smart Grid*, vol. 9, no. 3, pp. 2086–2096, May 2018.

[33] M. Koller, T. Borsche, A. Ulbig, and G. Andersson, "Defining a degradation cost function for optimal control of a battery energy storage system," in *Proc. IEEE Grenoble Conf.*, 2013, pp. 1–6.

[34] E. Ela and M. O'Malley, "Studying the variability and uncertainty impacts of variable generation at multiple timescales," *IEEE Trans. Power Syst.*, vol. 27, no. 3, pp. 1324–1333, Aug. 2012.

[35] E. A. Bakirtzis, P. N. Biskas, D. P. Labridis, and A. G. Bakirtzis, "Multiple time resolution unit commitment for short-term operations scheduling under high renewable penetration," *IEEE Trans. Power Syst.*, vol. 29, no. 1, pp. 149–159, Jan. 2014.

[36] E. A. Bakirtzis and P. N. Biskas, "Multiple time resolution stochastic scheduling for systems with high renewable penetration," *IEEE Trans. Power Syst.*, vol. 32, no. 2, pp. 1030–1040, Mar. 2017.

[37] H. Ding, P. Pinson, Z. Hu, and Y. Song, "Optimal offering and operating strategies for wind-storage systems with linear decision rules," *IEEE Trans. Power Syst.*, vol. 31, no. 6, pp. 4755–4764, Nov. 2016.

[38] Y. Wang, Y. Dvorkin, R. Fernández-Blanco, B. Xu, T. Qiu, and D. S. Kirschen, "Look-ahead bidding strategy for energy storage," *IEEE Trans. Sustain. Energy*, vol. 8, no. 3, pp. 1106–1117, Jul. 2017.

[39] E. B. Ssekulima, M. B. Anwar, A. Al-Hinai, and M. S. El-Moursi, "Wind speed and solar irradiance forecasting techniques for enhanced renewable energy integration with the grid: A review," *IET Renewable Power Gener.*, vol. 10, no. 7, pp. 885–898, Jul. 2016.

[40] M. Khalid, M. AlMuhaini, R. P. Aguilera, and A. V. Savkin, "Method for planning a wind/solar/battery hybrid power plant with optimal generation-demand matching," *IET Renewable Power Gener.*, vol. 12, no. 15, pp. 1800–1806, 2018.

[41] L. Pinto, J. Szczupak, and L. Nogueira, "An optimal less vulnerable renewable portfolio," in *Proc. IEEE Int. Energy Conf.*, 2014, pp. 340–345.

[42] M. Alsayed, M. Cacciato, G. Scarcella, and G. Scelba, "Multicriteria optimal sizing of photovoltaic-wind turbine grid connected systems," *IEEE Trans. Energy Convers.*, vol. 28, no. 2, pp. 370–379, Jun. 2013.

[43] M. B. Anwar, M. S. El Moursi, and W. Xiao, "Novel power smoothing and generation scheduling strategies for a hybrid wind and marine current turbine system," *IEEE Trans. Power Syst.*, vol. 32, no. 2, pp. 1315–1326, Mar. 2017.

[44] C. A. Correa, A. Gerossier, A. Michiorri, and G. Kariniotakis, "Optimal scheduling of storage devices in smart buildings including battery cycling," in *Proc. IEEE Manchester PowerTech*, 2017, pp. 1–6.

[45] S. Pfenninger and I. Staffell, "Renewables Ninja," 2016. [Online]. Available: https://www.renewables.ninja/

[46] O. El-Dakkak, S. Feng, M. Wahbah, T. H. M. EL-Fouly, and B. Zahawi, "Combinatorial method for bandwidth selection in wind speed kernel density estimation," *IET Renewable Power Gener.*, vol. 13, no. 10, pp. 1670–1680, 2019.

[47] M. Wahbah, S. Feng, T. H. M. EL-Fouly, and B. Zahawi, "Root-transformed local linear regression for solar irradiance probability density estimation," *IEEE Trans. Power Syst.*, vol. 35, no. 1, pp. 652–661, Jan. 2020.

[48] A. W. Bowman, "An alternative method of cross-validation for the smoothing of density estimates," *Biometrika*, vol. 71, no. 2, pp. 353–360, 1984.

[49] Vestas v82-1.5, Accessed: Apr. 5, 2020. [Online]. Available: https://en.wind-turbine-models.com/turbines/1727-vestas-v82-1.5

[50] Y. M. Atwa, E. F. El-Saadany, M. M. A. Salama, and R. Seethapathy, "Optimal renewable resources mix for distribution system energy loss minimization," *IEEE Trans. Power Syst.*, vol. 25, no. 1, pp. 360–370, Feb. 2010.

[51] B. Mohandes, S. Acharya, M. S. E. Moursi, A. S. Al-Sumaiti, H. Doukas, and S. Sgouridis, "Optimal design of an islanded microgrid with load shifting mechanism between electrical and thermal energy storage systems," *IEEE Trans. Power Syst.*, vol. 35, no. 4, pp. 2642–2657, Jul. 2020.

[52] Y. Dvorkin, Y. Wang, H. Pandzic, and D. Kirschen, "Comparison of scenario reduction techniques for the stochastic unit commitment," in *Proc. IEEE PES Gen. Meeting, Conf. Expo.*, 2014, pp. 1–5.

[53] R. J. Bessa, V. Miranda, A. Botterud, Z. Zhou, and J. Wang, "Time-adaptive quantile-copula for wind power probabilistic forecasting," *Renewable Energy*, vol. 40, no. 1, pp. 29–39, 2012. [Online]. Available: http://www.sciencedirect.com/science/article/pii/S0960148111004587

[54] R. Becker, "Generation of time-coupled wind power infeed scenarios using pair-copula construction," *IEEE Trans. Sustain. Energy*, vol. 9, no. 3, pp. 1298–1306, Jul. 2018.

[55] N. Haque, A. Tomar, P. Nguyen, and G. Pemen, "Dynamic tariff for day-ahead congestion management in agent-based LV distribution networks," *Energies*, vol. 13, no. 2, pp. 1–16, 2020.

[56] N. Littlestone and M. K. Warmuth, "The weighted majority algorithm," *Inf. Comput.*, vol. 108, pp. 212–261, 1994.

[57] J. Liu and O. Teytaud, "Scenario-based decision-making for power system investment planning," 2016, *arXiv:1607.01313*.

[58] R. Fu, D. Feldman, and R. Margolis, "U.S. solar photovoltaic system cost benchmark: Q1 2018," Nat. Renewable Energy Lab., Tech. Rep. NREL/TP-6A20-72399, Nov. 2018. [Online]. Available: https://www.nrel.gov/docs/fy19osti/72399.pdf

[59] Statista, *Electricity Prices for Households in France from 2010 to 2018, Semi-Annually*, Accessed: Oct. 6, 2020. [Online]. Available: https://www.statista.com/statistics/418087/electricity-prices-for-households-in-france/

[60] P. Manganiello, M. Balato, and M. Vitelli, "A survey on mismatching and aging of PV modules: The closed loop," *IEEE Trans. Ind. Electron.*, vol. 62, no. 11, pp. 7276–7286, Nov. 2015.

[61] T. Stehly, P. B. D. Heimiller, and G. Scott, "2017 cost of wind energy review," Nat. Renewable Energy Lab., Tech. Rep. NREL/TP-6A20-72167, Sep. 2018. [Online]. Available: https://www.nrel.gov/docs/fy18osti/72167.pdf

[62] R. D. Zimmerman, C. E. Murillo-Sanchez, and R. J. Thomas, "MAT-POWER: Steady-state operations, planning, and analysis tools for power systems research and education," *IEEE Trans. Power Syst.*, vol. 26, no. 1, pp. 12–19, Feb. 2011.

**Baraa Mohandes** (Member, IEEE) received the B.Sc. degree in electrical engineering from the Petroleum Institute, Khalifa University, UAE, in 2010, the M.Sc. degree from Khalifa University in 2015, and the Ph.D. degree in interdisciplinary engineering for his work on power systems optimization and economics in 2020. From 2010 to 2015, he was a Technical Support and Projects Engineer in one of the ADNOC's subsidiaries with the oil & gas industry. Following the completion of the Ph.D., he joined the Luxembourg Institute of Science and Technology (LIST) as a Postdoctoral Research Associate. His research interests include diverse, and include feedback control systems, and power system applications of data science, optimization, complex networks theory, and game-theory. He was the recipient of the Abu-Dhabi National Oil Company's (ADNOC) Scholarship from the Petroleum Institute, Khalifa University. In 2016, he was awarded the Masdar Institute's (MI) Fellowship for the joint MI and Massachusetts Institute of Technology Program. He was the recipient of a number of student awards.
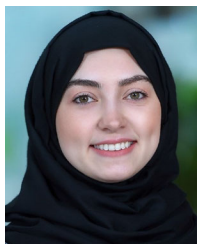
**Maisam Wahbah** (Member, IEEE) received the B.Sc., M.Sc., and Ph.D. degrees in electrical and computer engineering from Khalifa University, Abu Dhabi, UAE, in 2013, 2015, and 2019, respectively. Her M.Sc. research project focused on designing an efficient power conversion circuit for the piezo electric energy harvester as part of a fully-autonomous biomedical system. During her Ph.D. research, she focused on developing accurate and reliable statistical models of wind speed and solar irradiance resources for long-term power system planning and design studies. She is currently a Postdoctoral Fellow with Healthcare Engineering Innovation Center, the Department of Biomedical Engineering, Khalifa University. Her current research interests include biomedical signal analysis, nonparametric statistical modeling, and circuits and systems.

**Mohamed Shawky El Moursi** (Senior Member, IEEE) received the B.Sc. and M.Sc. degrees in electrical engineering from Mansoura University, Mansoura, Egypt, and the Ph.D. degree in electrical engineering from the University of New Brunswick (UNB), Fredericton, NB, Canada, in 1997, 2002, and 2005, respectively. From 2002 to 2005, he was a Research and Teaching Assistant with the Department of Electrical and Computer Engineering, UNB. He joined McGill University, Montreal, QC, Canada as a Postdoctoral Fellow with the Power Electronics Group. He joined Vestas Wind Systems, Arhus, Denmark, in the Technology R&D with the Wind Power Plant Group. He was with TRANSCO, Abu Dhabi, UAE, as a Senior Study and Planning Engineer. He is currently a Professor with the Electrical and Computer Engineering Department, Khalifa University of Science and Technology–Masdar Campus, Abu Dhabi, UAE and seconded to a Professor Position with the Faculty of Engineering, Mansoura University, Mansoura, Egypt and currently on leave. He was a Visiting Professor with the Massachusetts Institute of Technology, Cambridge, MA, USA. He is currently the Editor of the IEEE TRANSACTIONS ON POWER DELIVERY, the IEEE TRANSACTIONS ON POWER SYSTEMS, an Associate Editor for the IEEE TRANSACTIONS ON POWER ELECTRONICS, a Guest Editor of the IEEE TRANSACTIONS ON ENERGY CONVERSION, Guest Editor-in-Chief for special section between IEEE TRANSACTIONS ON POWER DELIVERY and IEEE TRANSACTIONS ON POWER SYSTEMS, Editor for the IEEE POWER ENGINEERING LETTERS, Regional Editor for *IET Renewable Power Generation* and Associate Editor of *IET Power Electronics Journals*. His research interests include power system, power electronics, FACTS technologies, VSC-HVDC systems, microgrid operation and control, renewable energy systems (Wind and PV) integration, and interconnections.
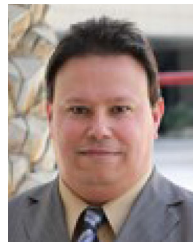
**Tarek H.M. EL-Fouly** (Senior Member, IEEE) received the B.Sc. and M.Sc. degrees from Ain Shams University, Cairo, Egypt, and the Ph.D. degree in electrical engineering from the University Of Waterloo, Waterloo, ON, Canada, in 1996, 2002, and 2008, respectively. In 2008, he joined CanmetENERGY, Natural Resources Canada, Government of Canada, as a Transmission and Distribution Research Engineer. In 2010, he was appointed as an Adjunct Assistant Professor with Electrical and Computer Engineering Department, the University of Waterloo. In 2014, he was promoted to Smart Microgrids Research Manager with CanmetENERGY, Natural Resources Canada. In January 2015, he joined the Khalifa University of Science and Technology as an Assistant Professor with Electrical and Computer Engineering Department and in July 2019, he got promoted to Associate Professor. He conducts research on smart grids, microgrids, high penetration of renewable energy resources, and integration of electrical energy storage systems.